To appear in: *SIAM Journal on Applied Dynamical Systems* (accepted on 23 February 2017)

Transport between two fluids across their mutual flow interface: the streakline approach*

Sanjeeva Balasuriya†

Abstract. Mixing between two different fluids with a mutual interface must be initiated by fluid transporting across this fluid interface, caused for example by applying an unsteady velocity agitation. In general, there is no necessity for this physical flow barrier between the fluids to be associated with extremal or exponential attraction as might be revealed by applying Lagrangian coherent structures, finite-time Lyapunov exponents or other methods on the fluid velocity. It is shown that streaklines are key to understanding the breaking of the interface under velocity agitations, and a theory for locating the relevant streaklines is presented. Simulations of streaklines in a cross-channel mixer and a perturbed Kirchhoff's elliptic vortex are quantitatively compared to the theoretical results. Additionally, a methodology for quantifying the unsteady advective transport between the two fluids using streaklines is presented, and verified numerically for the same two examples.

Key words. Flow interface, two-phase fluids, fluid mixing, interfacial transport

AMS subject classifications. 76T99, 37C60, 76R05, 34E99, 34A26

1. Introduction.

If present in a steady nonchaotic flow, coherent blobs of two miscible fluids separated by a streamline will tend to mix together via the typically inefficient mechanism of diffusion. This is a common situation in microfluidics, in which a sample and a reagent are to be mixed in order to achieve a biochemical reaction in, say, a DNA synthesis experiment, and in which low Reynolds numbers are inevitable due to spatial dimensions and typical velocity scales. Accelerating the mixing can be achieved by introducing unsteady velocity agitations to impart advective transport across the flow interface. If this process results in fluid filamentation across/near the interface, it will enhance diffusive mixing in addition to causing advective intermingling between the two fluids. Understanding this process, and being able to quantify resulting fluid mixing, is important in flows ranging from geophysical to microfluidic, for example in assessing how an introduced pollutant mixes with exterior fluid in the ocean, or how a sample and a reagent can be mixed together effectively in micro- or nano-level bioreactors.

For this two-fluid problem, the well-established tools of Lagrangian coherent structures [28, 45, 13] are inapplicable, as highlighted by simple examples in Fig. 1. In (a), two different fluids enter a microchannel from the left, each entering perhaps from syringes or tubes (not pictured) positioned on the upper and lower sides of the channel. Since these fluids could for example be a sample and a reagent in a microfluidic bioreactor, there is no necessity for the two fluids to be needed in the same proportion. Often, the fluids are rheologically similar (e.g., are both aqueous, but with different chemical solutes) and miscible. However, since the tiny dimensions

*Submitted to the editors: February 24, 2017.

Funding: This work was funded by the Australian Research Council through grant FT130100484.

†School of Mathematical Sciences, University of Adelaide, Adelaide SA 5005, Australia (sanjeevabalasuriya@yahoo.com, http://www.maths.adelaide.edu.au/sanjeeva.balasuriya/).

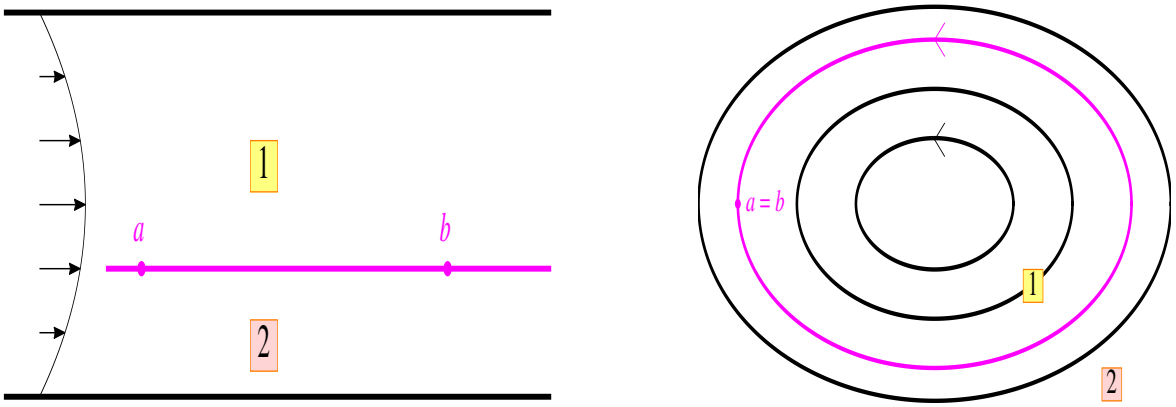

(a) channel flow (b) vortex blob

Figure 1. *Two situations in which a steady flow interface cannot be characterized in terms of a distinguished entity of* $\dot{\boldsymbol{x}} = \boldsymbol{u}(\boldsymbol{x})$*, but is rather the interface [magenta] between fluids* 1 *and* 2*.*

of microchannels are such that low Reynolds number flow is inevitable, the fluids will flow to the right in a laminar fashion, with their mutual fluid interface not along the centerline of the channel. Attempting to identify the flow interface *purely from the fluid velocity* is futile; there is absolutely nothing distinguished about the streamline along the flow interface (in magenta) in comparison to other streamlines. It is not even the streamline of maximum speed, which (if assuming the classical parabolic velocity profile) is at the centerline[1]. The flow interface is something *physical*, and not derivable *only* from the velocity field by performing standard Lagrangian coherent structure and related computations. For example, there is no necessity for the interface to be associated with extremal attraction or anomalously large exponential stretching, compared to nearby curves. Fig. 1(b) shows a situation in which a solute (a pollutant, nutrient, chemical, plume of higher temperature, etc) has intruded into the center of a vortex, requiring the interior fluid to be thought of as different from the exterior. The flow interface between the interior and exterior fluids here is a streamline, but once again there is nothing distinguished about this streamline based on the velocity field. There are closed streamlines both inside and outside this particular interface which distinguishes between the inside and outside fluids. It is such flow interfaces between miscible fluids, and determining transport between the two fluids after the introduction of velocity agitations, that is the focus of this article.

Studying interfaces between two miscible fluids is not new, and includes much recent work [27, 66, 57, 25, 38, 65, 22, 49]. The approach followed here, in which the Lagrangian particle evolution is directly used in conjunction with techniques inspired by dynamical systems theory, is however a novel approach, which moreover provides tools for answering the questions posed above. The key to proceeding is in determining how one might identify the flow interface

[1]Local maxima of the speed are defined by Haller as 'parabolic Lagrangian Coherent Structures,' for which a theory has been developed [28].

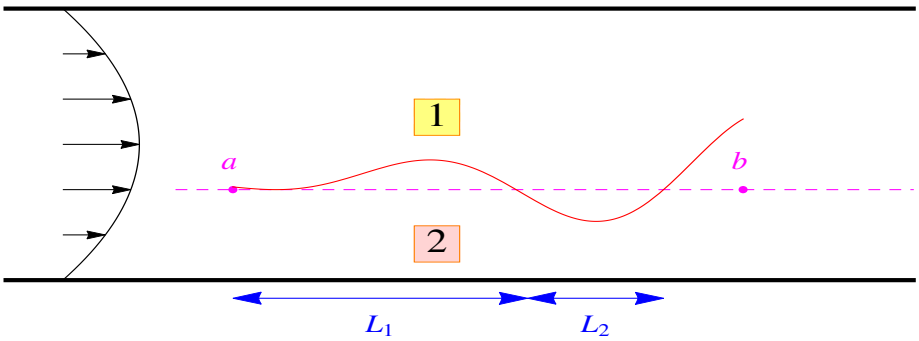

Figure 2. *The fluid interface [red] at an instance in time for the scenario in Fig. 1(a) after the addition of an unsteady velocity agitation operating between* $\boldsymbol{a}$ *and* $\boldsymbol{b}$*, with the steady (non-agitated) interface shown by the dashed magenta line.*

under unsteady velocity agitations. It will be argued that the concept of a *streakline* is the most appropriate to use, under the condition that the velocity agitation is confined to a certain region. A streakline is defined to be the set of points which have gone through a chosen fixed point at some instance in the past, and would experimentally be obtained by releasing dye continuously from a fixed location [18, 63, 30]. (The streaklines used here are *not* associated with stable/unstable manifolds, as might be the case if considering the interface between a fluid and a bluff body [47, 51, 68, 2].) A brief explanation as to why streaklines are important is because if the agitation is confined to being downstream of $\boldsymbol{a}$ Fig. 1(a), then the streakline passing through $\boldsymbol{a}$ will demarcate the boundary between the two fluids, as fluids arriving from upstream on the two sides of $\boldsymbol{a}$ are different. In other words, the interface between the two fluids can be identified in terms of a streakline.

Determining the time-evolution of streaklines due to unsteady velocity agitations shall be the first focus of this article. Section 2 will develop the theory for the streakline—the 'nominal' flow interface when the weak velocity agitations are considered—and its evolution with time. Explicit analytical expressions are obtained by utilizing dynamical systems methods, and are valid for general time-dependence in the velocity agitation, and also allow for compressibility in the fluid. Section 3 provides a validation of these expressions in comparison to numerical simulations of streaklines, in two examples which are loosely based on Fig. 1. Specifically, the first example considers the impact on the flow interface of introducing flow in cross-channels (a so-called cross-channel micromixer [21, 20, 44, 58, 34, 11]), while the second concerns the impact on the 'boundary' of Kirchhoff's elliptic vortex [32, 61, 41, 26, 39] due to weak external strain.

The second focus of this article is to make sense of *transport* which eventually leads to mixing between the two fluids. This presumably has a connection to how the fluid interface between them is evolving, but what is it? Consider for example Fig. 2, which is associated with an unsteady velocity agitation for the channel flow situation of Fig. 1(a). The agitation can be a result, for example, of applying a time-varying cross-flow to the main channel via syringes/cross-channels/boundary-pulsation/electromagnetic forces/corrugations [21, 58, 34, 11, 19, 1, 55]; this is not shown in the figure. The red curve is the flow interface in the (now

unsteady) flow at some fixed instance in time, while the dashed magenta curve is the original (steady) flow interface for the situation in which there is no additional agitation. Now, the (red) interface will be evolving as Lagrangian curve (i.e., a *timeline*) under unsteady velocity agitations, and therefore there can be no Lagrangian fluid flux across it. Thus, thinking of the interface as an entity which evolves in a Lagrangian sense is not helpful in attempting to capture fluid exchange. Is the answer, then, to use an Eulerian definition of an interface, and quantify transport across it? The obvious candidate for such a fixed Eulerian curve in this example is the original flow interface, the dashed magenta curve in Fig. 2. Integrating the instantaneous normal velocities along this defines an Eulerian fluid flux. Bear in mind, however, that the fluid interface (in the sense of the boundary between the two fluids) is moving with time, and would be at an instance in time something like the red curve in Fig. 2. Therefore the (fixed in time) magenta curve is sometimes within fluid 2, and sometimes within fluid 1. So if computing the Eulerian flux across the magenta line, in some instances one would be quantifying the transport from fluid 2 to fluid 2 (in region L_1, say), and in other instances from fluid 1 to fluid 1 (in region L_2). The fact that fluid 2 has crossed the magenta line in region L_1 does not by itself mean that when viewed downstream, this will result in there being fluid 2 in the upper (nominally fluid 1) region, since the streakline can dip down again. In other words, there is no guarantee that using such an Eulerian approach would capture the *interchange* of fluids.

The above discussion points to the necessity of being able to understand 'transport between the two fluid regions,' as a mechanism for achieving mixing between the two fluids. As is well-known, unsteady advection (also sometimes called *stirring*) can result in well-mixed fluids [3, 55, 11]. In this instance, this can be thought of as the intermingling between fluids 1 and 2 which is eventually achieved when examining the fluid far downstream of $\boldsymbol{b}$, where only the advective process given by $\dot{\boldsymbol{x}} = \boldsymbol{u}(\boldsymbol{x}, t)$ is considered. Section 4 shows how the streakline can be used to define a relevant time-varying transport. Since as has been already argued, a purely Lagrangian or purely Eulerian approach has difficulties, a *hybrid* method which encapsulates the origins and destinations of fluid particles is formulated. An explicit approximation for the time-varying transport is obtained; this shall be useful in future work in, for example, determining forms of velocity agitations which maximize transport (as in the similar developments for heteroclinic situations [6, 4, 8, 15]). The theory is once again validated by numerical simulations of the same two examples in Section 5. The second of these offers a novel way of examining the oft-studied problem of vortices in an external straining field [48, 31, 24, 40, 35, 43, 60, 17, 67, 33]; here, the Lagrangian fluid interchange between the interior and exterior fluids caused by weak external strain is quantified. Finally, directions of future work are outlined in Section 6.

2. Streaklines.

Consider a steady two-dimensional flow in which there is a persistent (one-dimensional) flow interface between two different fluids. The goal is to understand how an *unsteady* velocity agitation affects this flow interface, and how the resulting advective transport between the fluids can be quantified. Firstly, to introduce notation, consider the steady flow

$$\dot{\boldsymbol{x}} = \boldsymbol{u}(\boldsymbol{x}) \quad , \quad \boldsymbol{x} \in \mathbb{R}^2 \, . \tag{1}$$

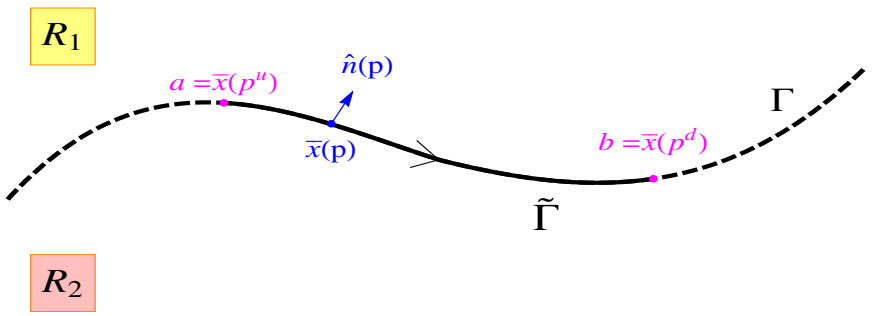

Figure 3. *The generic steady streakline* Γ *[dashed], and its restriction* $\tilde{\Gamma}$ *[solid] between* $\boldsymbol{a}$ *and* $\boldsymbol{b}$*, which is parametrized in the form* $\bar{\boldsymbol{x}}(p)$*, with* $p \in [p^{\mathrm{u}}, p^{\mathrm{d}}]$*.*

Incompressibility is *not* assumed for the fluids, but $\boldsymbol{u}$ is assumed to be smooth. Now, a flow interface Γ that persists in the steady flow (1) must have no fluid velocity perpendicular to Γ. Thus, the velocity $\boldsymbol{u}$ is tangential to Γ, which can be characterized as part of a streamline of the initial steady flow. Since the velocity is steady, this can be thought of as a streamline, streakline, or pathline, but as shall be seen shortly, using the *streakline* concept allows the correct generalization to an unsteady flow. Let Γ be such a streakline. A velocity agitation will only be applied to the part $\tilde{\Gamma}$ of Γ which lies between the points $\boldsymbol{a}$ and $\boldsymbol{b}$. Thus, $\tilde{\Gamma}$ is a curve which starts at the upstream anchor point $\boldsymbol{a}$, and connects along the streakline emanating from $\boldsymbol{a}$ and progressing to the downstream anchor point $\boldsymbol{b}$. Two generic situations are possible: (i) $\boldsymbol{a} \neq \boldsymbol{b}$, in which case $\tilde{\Gamma}$ is an open curve, and (ii) $\boldsymbol{a} = \boldsymbol{b}$, in which case $\tilde{\Gamma}$ is a closed curve. These two situations are exactly analogous to the topological structures in Fig. 1. It is clear that in the open case Γ extends beyond $\tilde{\Gamma}$, while in the closed case, Γ retraces the closed loop $\tilde{\Gamma}$ repeatedly.

There are two assumptions on the flow interface. The first is that $\tilde{\Gamma}$ be a *simple* (non self-intersecting) curve. The second—which is crucial—is that $\boldsymbol{u} \neq \boldsymbol{0}$ on Γ. If $\boldsymbol{u} = \boldsymbol{0}$ at some points on Γ, then Γ will consist of parts of heteroclinic manifolds, and established theory for locating these [9, 10, 13], and the resulting transport in time-periodic [48, 64, 5], aperiodic [7] or impulsive [14] situations, applies. Moreover, standard diagnostic tools such as finite-time Lyapunov exponents or curves of maximal attraction are viable candidates for numerically determining the flow barriers. Therefore, stagnation points will be explicitly precluded on Γ; it shall be *non-heteroclinic*.

The streakline Γ is easily defined as a curve in $\mathbb{R}^2$ via a parametrization $\bar{\boldsymbol{x}}(p)$ as shown in Fig. 3. Here $\bar{\boldsymbol{x}}(p)$ is a solution to (1)—where the parameter p can be thought of as time—which obeys $\bar{\boldsymbol{x}}(p^{\mathrm{u}}) = \boldsymbol{a}$ and $\bar{\boldsymbol{x}}(p^{\mathrm{d}}) = \boldsymbol{b}$. The superscript u is to be identified with '*u*pstream,' and d with '*d*ownstream' throughout this article. Here, Γ is to be thought of as the extension beyond $\boldsymbol{a}$ and $\boldsymbol{b}$, which therefore provides the boundary between the two different fluid regions denoted by R_1 and R_2. The restriction $p \in [p^{\mathrm{u}}, p^{\mathrm{d}}]$ identifies $\tilde{\Gamma}$, the part lying between $\boldsymbol{a}$ and $\boldsymbol{b}$, to which the velocity agitation will be confined. If $\tilde{\Gamma}$ is closed, then the velocity agitation will occur throughout Γ (the periodic repetition of $\tilde{\Gamma}$), except at the anchor point $\boldsymbol{a} = \boldsymbol{b}$. Indeed,

$\bar{\boldsymbol{x}}(p)$ is a periodic function of p in this instance, but the restriction to $\tilde{\Gamma}$ achieved by setting $p \in [p^{\mathrm{u}}, p^{\mathrm{d}}]$ implies that $\bar{\boldsymbol{x}}(p^{\mathrm{u}}) = \boldsymbol{a}$ but that p^{d} is the next instance in which $\bar{\boldsymbol{x}}(p)$ reaches $\boldsymbol{a}$, which is of course $\boldsymbol{b}$. In either the open or closed situation, of interest is the fact that the *upstream streakline* emanating from $\boldsymbol{a}$ directly hits $\boldsymbol{b}$. This defines Γ as a clear separator between the regions R_1 and R_2, occupied respectively by fluids 1 and 2.

The principal focus is the streakline generated by continually releasing dye from $\boldsymbol{a}$, whose time-variation can be quantified by the definition

$$\Gamma_0(t) := \bigcup_{p \geq p^{\mathrm{u}}} \{\boldsymbol{x}_0^{\mathrm{u}}(p,t) \text{ which solves } (1) \text{ with condition } \boldsymbol{x}_0^{\mathrm{u}}(p, t-p+p^{\mathrm{u}}) = \boldsymbol{a}\} \,. \tag{2}$$

The p above provides a parametrization of the upstream streakline at each fixed time instance t, where the p can be thought of as *identifying a particle*. The particle which is at the location $\bar{\boldsymbol{x}}(p)$ at time t is the one which passed through $\boldsymbol{a}$ at time $t - p + p^{\mathrm{u}}$ (i.e., a time $p^{\mathrm{u}} - p$ prior to t). Note that the upstream streakline here is not restricted to $\tilde{\Gamma}$, since the p-values may go beyond p^{d}. However $p \geq p^{\mathrm{u}}$ restricts the streakline to being downstream of $\boldsymbol{a}$.

The parametrization above—with p being a fixed *p*article along the streakline and t the *t*ime at which the streakline is being observed—shall be retained when the flow is subject to an unsteady velocity agitation in the form

$$\dot{\boldsymbol{x}} = \boldsymbol{u}\,(\boldsymbol{x}) + \boldsymbol{v}\,(\boldsymbol{x}, t) \,. \tag{3}$$

in which the agitation $\boldsymbol{v}$ is restricted to obey

$$\boldsymbol{v}(\bar{\boldsymbol{x}}(p), t) = \begin{cases} 0 \quad \text{for } p \leq p^{\mathrm{u}} \text{ or } p \geq p^{\mathrm{d}} & (\text{open } \tilde{\Gamma}) \\ 0 \quad \text{when } \bar{\boldsymbol{x}}(p) = \boldsymbol{a} & (\text{closed } \tilde{\Gamma}) \end{cases} \,. \tag{4}$$

For open $\tilde{\Gamma}$ this means that the unsteady agitation $\boldsymbol{v}$ is zero up to (and including) the point $\boldsymbol{a}$, which enables the understanding that the $\boldsymbol{a}$ remains at the interface of the two fluids. Thus, $\boldsymbol{a}$ continues to be an anchor point on the flow interface in forward time. For closed $\tilde{\Gamma}$, $\boldsymbol{a} = \boldsymbol{b}$, and $\bar{\boldsymbol{x}}(p)$ periodically traverses $\tilde{\Gamma}$. Thus, once going 'beyond' $\boldsymbol{b}$ on $\tilde{\Gamma}$, one returns to points in which a velocity agitation continues to exist, and it cannot be 'turned off' as in the open situation. Moreover— in representing this as an agitation on a dominant steady flow—it shall be assumed that

$$|\boldsymbol{v}\,(\boldsymbol{x}, t)| \leq \varepsilon\,|\boldsymbol{u}\,(\boldsymbol{x})| \quad \text{for } \boldsymbol{x} \in \Gamma \text{ and } t \in \mathbb{R} \,,$$

where $\varepsilon \ll 1$, and $\boldsymbol{v}$ is smooth in $\boldsymbol{x}$. Note however that $\boldsymbol{v}$ is otherwise arbitrary for the theory to follow: it may satisfy $\boldsymbol{\nabla} \cdot \boldsymbol{v} \neq 0$, possess aperiodic time-dependence, etc. Now, exactly analogous to the definitions of the steady streakline, the *unsteady* streakline for the flow (3) can be defined by

$$\Gamma_\varepsilon^{\mathrm{u}}(t) := \bigcup_{p \geq p^{\mathrm{u}}} \{\boldsymbol{x}_\varepsilon^{\mathrm{u}}(p,t) \text{ which solves } (3) \text{ with condition } \boldsymbol{x}_\varepsilon^{\mathrm{u}}(p, t-p+p^{\mathrm{u}}) = \boldsymbol{a}\} \,. \tag{5}$$

The streakline at a fixed time t are shown in Fig. 4, to be viewed in conjunction with the steady (non-agitated) streakline picture of Fig. 3. The steady Γ of Fig. 4 is shown by the thick

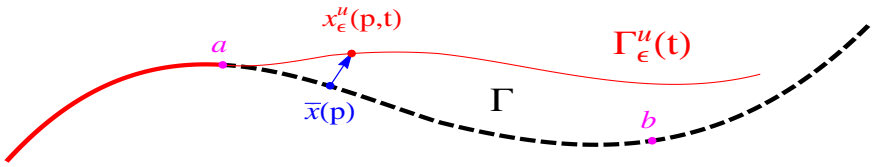

Figure 4. *The unsteady streakline $\Gamma^{\mathrm{u}}_\varepsilon(t)$ [red] at an instance in time t, defined according to (5).*

curves: it consists of the thick red curve upstream of $\boldsymbol{a}$, and is continued by the thick dashed black curve extending beyond $\boldsymbol{b}$. The unsteady steakline $\Gamma^{\mathrm{u}}_\varepsilon(t)$ is shown in red, and consists of a thick part which coincides with Γ (upstream of $\boldsymbol{a}$), and then the extension which need not. As time progresses, (the thin portion of) $\Gamma^{\mathrm{u}}_\varepsilon(t)$ will wiggle around due to the velocity agitation.

In preparation for stating the characterization of the unsteady streaklines, the notation

$$J := \begin{pmatrix} 0 & -1 \\ 1 & 0 \end{pmatrix}$$

will be useful. Notice that J rotates vectors by $+\pi/2$, and from Fig. 3,

$$\hat{\boldsymbol{n}}(p) := \frac{J\boldsymbol{u}\left(\bar{\boldsymbol{x}}(p)\right)}{\left|\boldsymbol{u}\left(\bar{\boldsymbol{x}}(p)\right)\right|} \tag{6}$$

is a unit normal vector to Γ at the parametric location p. The unsteady modifications to the streakline in this normal direction can now be quantified:

Theorem 1 (Streakline approximation). *For $p \in [p^{\mathrm{u}}, P]$ for any finite P, the parametric representation $\boldsymbol{x}^{\mathrm{u}}_\varepsilon(p,t)$ of $\Gamma^{\mathrm{u}}_\varepsilon(t)$ satisfies*

$$[\boldsymbol{x}^{\mathrm{u}}_\varepsilon(p,t) - \bar{\boldsymbol{x}}(p)] \cdot \hat{\boldsymbol{n}}(p) = \frac{M^{\mathrm{u}}(p,t)}{\left|\boldsymbol{u}\left(\bar{\boldsymbol{x}}(p)\right)\right|} + \mathcal{O}(\varepsilon^2) \tag{7}$$

where

$$M^{\mathrm{u}}(p,t) := \int_{p^{\mathrm{u}}}^{p} \exp\left[\int_{\tau}^{p} \left[\boldsymbol{\nabla}\cdot\boldsymbol{u}\right]\left(\bar{\boldsymbol{x}}(\xi)\right) \mathrm{d}\xi\right] \left[J\boldsymbol{u}\left(\bar{\boldsymbol{x}}(\tau)\right)\right] \cdot \boldsymbol{v}\left(\bar{\boldsymbol{x}}(\tau), \tau + t - p\right) \mathrm{d}\tau\,. \tag{8}$$

For the proof, the reader is referred to Appendix A. The crux of this theorem is in characterizing the normal displacement from $\bar{\boldsymbol{x}}(p)$ to a point $\boldsymbol{x}^{\mathrm{u}}_\varepsilon(p,t)$ on $\Gamma^{\mathrm{u}}_\varepsilon(t)$, as indicated by the arrow in Fig. 4. This is therefore given by

$$\boldsymbol{x}^{\mathrm{u}}_\varepsilon(p,t) = \bar{\boldsymbol{x}}(p) + \frac{M^{\mathrm{u}}(p,t)}{\left|\boldsymbol{u}\left(\bar{\boldsymbol{x}}(p)\right)\right|}\hat{\boldsymbol{n}}(p) + \mathcal{O}(\varepsilon^2) \tag{9}$$

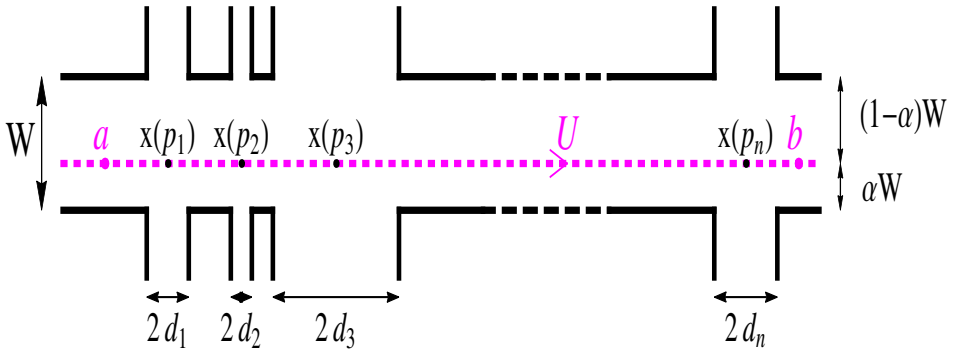

Figure 5. *Channel flow with cross-channels.*

if the tangential displacement is ignored[2]. This allows for finite extents of the streakline to be located and tracked theoretically to $\mathcal{O}(\varepsilon)$, since $M^{\mathrm{u}} = \mathcal{O}(\varepsilon)$ due to the presence of $\boldsymbol{v}$ in the integral (8).

If $\tilde{\Gamma}$ is open, the fact that $\boldsymbol{v}\,(\bar{\boldsymbol{x}}(p), \boldsymbol{.}) = \boldsymbol{0}$ for $p > p^{\mathrm{d}}$ means that the integrand is zero beyond p^{d}. No additional displacement is accrued by streaklines passing beyond $\boldsymbol{b}$. For closed $\tilde{\Gamma}$, however, $\boldsymbol{v}$ will return to being nonzero beyond $\boldsymbol{b} = \boldsymbol{a}$, and therefore the velocity agitation continues to cause an accumulation of displacement. In this case, the terms in (8) involving $\boldsymbol{u}$ will periodically repeat, but the presence of the general time-dependence in $\boldsymbol{v}$ in (8) ensures that the normal displacement is *not* generally periodic in p or t.

3. Streakline validation.

In this section, streaklines will be obtained by numerical simulation, and compared with the theoretical expressions derived previously, in two examples: two fluids in a channel, and an anomalous fluid inside an elliptic vortex. These same examples will be examined subsequently, in Section 5, in computing the associated fluid transport.

3.1. Two fluids in a microchannel.

As the first example, consider two incompressible fluids traveling along a straight channel. At the microfluidic level, it is well-known that these will tend not to mix across their flow interface, and sloshing fluid in the direction normal to this interface via cross-channels is a standard strategy which is used [21, 20, 44, 58, 34, 11]. This interface is shown by the dashed curve in Fig. 5, which need not be centered since the volume flow rates of the upper and lower fluids need not be the same. Consider a situation in which the interface splits the main channel, of width W, into the ratios $\alpha : 1-\alpha$, where $0 < \alpha < 1$. Assuming that the fluid on the interface will move at a constant speed U, and that the interface is at $y = 0$, for well-developed steady flow (with no flow in the cross-channels) the streamwise velocity would be

$$\boldsymbol{u}(x,y) = \frac{U}{\alpha(1-\alpha)}\left(1-\alpha-\frac{y}{W}\right)\left(\alpha+\frac{y}{W}\right)\hat{\boldsymbol{\imath}}\,. \tag{10}$$

[2]Ignoring the tangential displacement is reasonable in the sense that the streakline has p as its parameter varying in precisely the tangential direction, and when plotting $\boldsymbol{x}_\varepsilon^{\mathrm{u}}(p,t)$ for a range of p to obtain the streakline curve, any tangential displacement will be barely visible [9]. This is indeed reflected in the examples presented here. If needed, tangential displacements can be quantified [9], but this is unwieldy.

In the above, a parabolic profile is assumed based on experimental evidence [58, 44, 34, 8]. The steady streakline is therefore $\bar{\boldsymbol{x}}(\tau) = (x(\tau), 0) = (U\tau, 0)$. To account for the many possibilities which are available in the literature, a *general* geometry consisting of n cross-channels shall be assumed. The jth cross-channel is centered at the x location $x(p_j)$, and is assumed to have width $2d_j$, where for consistency it is necessary that $x(p_j) + d_j < x(p_{j+1}) - d_{j+1}$. In this case, $x(p_j) = Up_j$, and $\boldsymbol{a}$ and $\boldsymbol{b}$ can be taken to be any points on $y = 0$ upstream of $(Up_1 - d_1, 0)$ and downstream of $(Up_n + d_n, 0)$ repectively. Thus, $p^{\mathrm{u}} \le p_1 - d_1/U$ and $p^{\mathrm{d}} \ge p_n + d_n/U$. The cross-channel velocities can be modeled by

$$\boldsymbol{v}_j(x, y, t) = \frac{v_j}{d_j^2}\left[(x - Up_j)^2 - d_j^2\right]\cos(\omega t + \phi_j)\,\hat{\boldsymbol{j}}\,, \tag{11}$$

for $Up_j - d_j \le x \le Up_j + d_j$, where $v_j > 0$ is a velocity scale representing the speed at the center of the cross-channel, $\omega > 0$ is the frequency of fluid sloshing, and ϕ_j enables the specification of how the cross-channels are operating in relation to one another. For example, if all cross-channels are in phase, then $\phi_j \equiv 0$, and if adjacent ones are exactly out of phase, then $\phi_j = j\pi$. Therefore, the geometry and velocity specification can account for very general cross-channel configurations. It is assumed that $\varepsilon = \max_j |v_j| / U \ll 1$.

The observations $|\boldsymbol{u}| = U$, $\boldsymbol{\nabla}\cdot\boldsymbol{u} = 0$ and $J\boldsymbol{u} = U\hat{\boldsymbol{j}}$ on the interface are useful in computing the upstream streakline as given in (9). Thus, to leading-order

$$\boldsymbol{x}_\varepsilon^{\mathrm{u}}(p, t) = Up\,\hat{\boldsymbol{i}} + \frac{M_c^{\mathrm{u}}(p, t)}{U}\hat{\boldsymbol{j}}\,, \tag{12}$$

where, from (8), $M_c^{\mathrm{u}}(p, t)$ is nonzero only for $p > p_1 - d_1/U$, where it takes the value

$$M_c^{\mathrm{u}}(p, t) = \int_{p_1 - d_1/U}^{\min\{p, p_n + d_n/U\}} \sum_{j=1}^{n} \mathbb{I}_{[p_j - d_j/U,\, p_j + d_j/U]}(\tau)\, U\frac{v_j}{d_j^2}\left[U^2(\tau - p_j)^2 - d_j^2\right]\cos\left[\omega(\tau + t - p) + \phi_j\right]\mathrm{d}\tau\,. \tag{13}$$

(The subscript c is used for '$c$hannel,' to contrast with the vortex example to be presented subsequently.) For given parameter values, the integral above can be explicitly computed. To compare with numerics, choose a situation where $U = 1$, $\omega = 4$, $\varepsilon = 0.1$ and $n = 5$, with channels specified by $\{p_j\} = \{1, 2, 3, 4, 5\}$, $\{v_j\} = \varepsilon\{1, 0.5, 1, 1, 1\}$, $\{d_j\} = \{0.1, 0.1, 0.1, 0.3, 0.1\}$ and $\{\phi_j\} = \{\pi, 2\pi, 3\pi, 4\pi, 7\pi/2\}$. Thus, the second cross-channel has a smaller maximum speed than the others, the fourth is triple the width of the others, and the fifth has a phase which is at odds with the exactly-out-of-phase nature of the other channels. Now, the parameters W and α do not contribute to the theoretical solution (13), but are necessary for the numerical simulations; here, $W = 2$ and $\alpha = 1/3$ are used. Numerical simulations with red dye released at $\boldsymbol{a} = (0.5, 0)$ (upstream of velocity agitations) on the interface from time 0 onwards are shown in Fig. 6 at several instances in time by the red curves. The simulations are performed here by continuously releasing particles at $\boldsymbol{a}$ and tracking this stream of particles under the flow of the full velocity field to form a streakline. (An alternative method [63, 30] would be to identify streaklines at each time instance as being everywhere tangential to a modified vector field, but the more direct method following the definition of streaklines is used here.) The dashed black curves illustrate the instantaneous velocities in the cross directions, scaled so that they fit into this picture. It should be noted that beyond $(5.1, 0)$ (the final

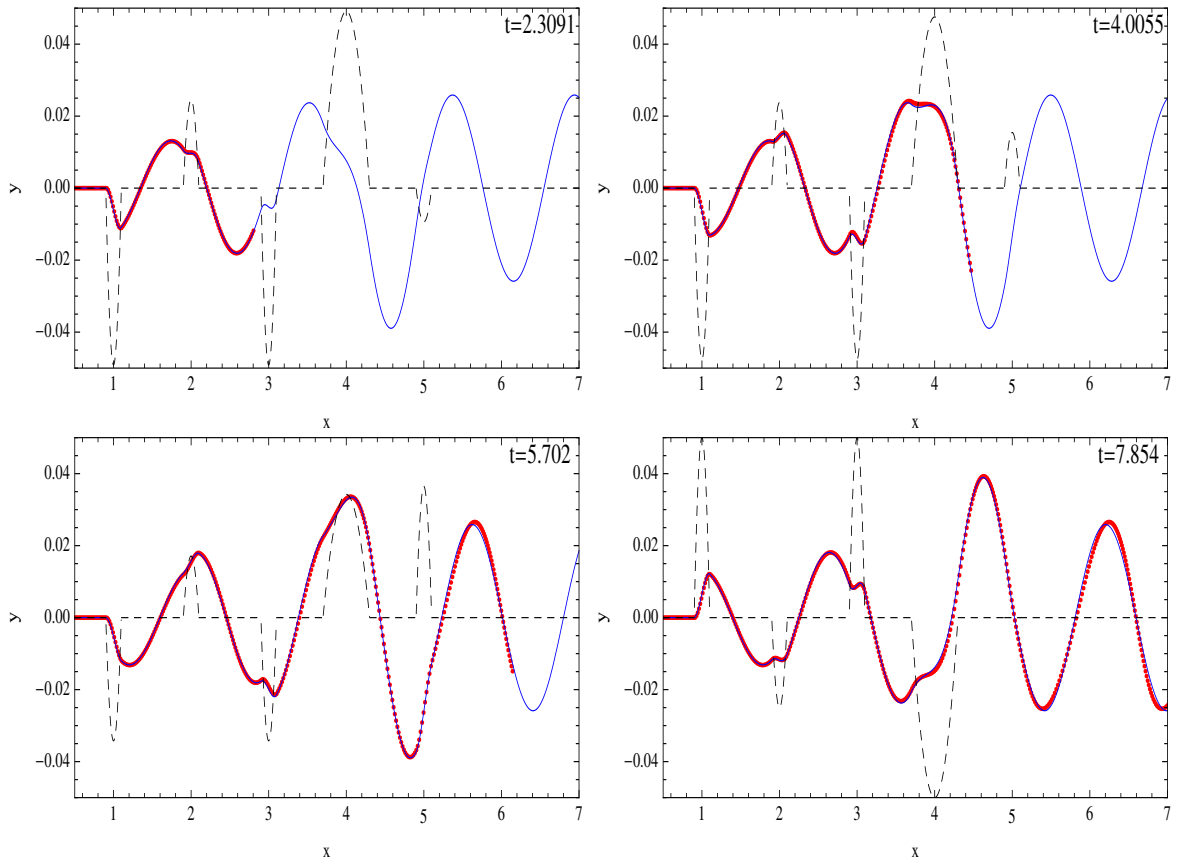

Figure 6. *Evolution of upstream streakline [red dots] for channel flow, with dye released on the fluid interface at* $(0.5, 0)$ *from time* 0 *onwards, with the instantaneous cross-velocity (with channel configuration as described in the text) shown by the dashed black curves. The blue curves are the approximate streaklines computed using (12) and (13), and the closeness between the red and blue curves is such that they are difficult to distinguish.*

point at which the velocity agitation applies) with these parameter values, the streakline is *not* simply along $y = 0$. The curves in the streakline caused by the velocity agitations will be swept along, with no additional agitation. A video of the upstream streakline (i.e., unsteady fluid interface) evolution is provided with the Supplementary Materials.

The blue curves in Fig. 6 are the *theoretical* leading-order streaklines, computed using (12) and (13)). The agreement between the red and blue curves is excellent, and indeed the two separate curves are difficult to distinguish in Fig. 6. One slight difference is that in the blue theoretical streakline extends all the way across. This is because the theoretical streakline has been computed by considering fluid particles going through $\boldsymbol{a} = (0.5, 0)$ at all times in the past. In contrast, the red numerical streaklines shown in Fig. 6 were obtained by synthetically releasing red dye at $\boldsymbol{a}$ from time 0 onwards, and thus the streaks are gradually extending towards the right as time progresses. While making a decision of this sort is inevitable in a numerical simulation, the theoretical expressions enable the *full* streakline, associated with particles released at $\boldsymbol{a}$ in the distant past, to be obtained.

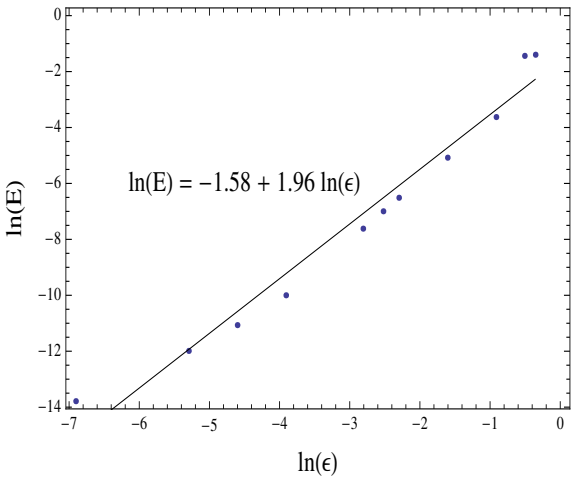

Figure 7. *The variation of the error between the numerically simulated and the explicit approximation (at* $x = 6.5$ *and* $t = 5(2\pi/\omega)$*) with* ε *[dots] for the cross-channel micromixer, in a log-log plot.*

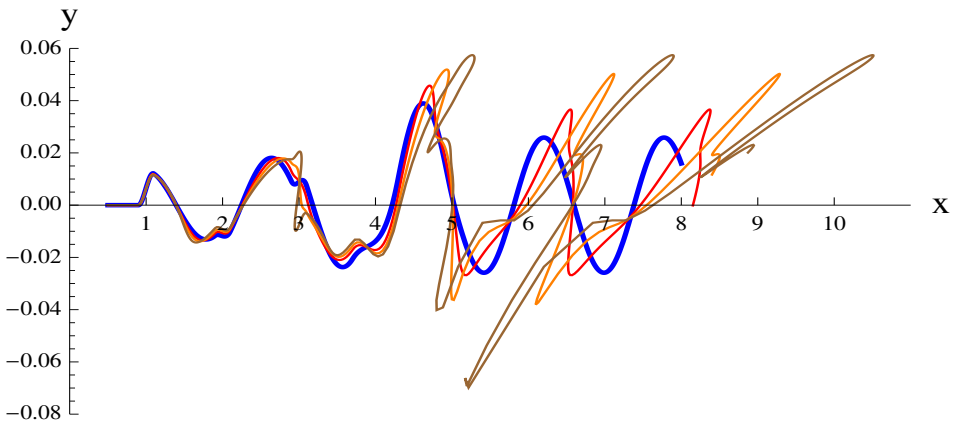

Figure 8. *The theoretical streakline [blue] at time* $5(2\pi/\omega)$ *with the same parameter values as in Fig. 6, compared with numerically simulated streaklines with* $\alpha = 0.1$ *[red],* 0.06 *[orange] and* 0.04 *[brown].*

The final panel in Fig. 6 is at a time corresponding to five times the period $2\pi/\omega$ of the flow. The error at this time is investigated in Fig. 7, in which the error between the numerical and explicit streaklines is computed at $x = 6.5$. A pointwise error computation is chosen here to be consistent with Theorem 1. Fig. 7 was determined by computing the error across a range of ε, and presenting the results in a log-log plot. The linear fit in the plot indicates that the error goes as $\varepsilon^{1.96}$, which is close to the $\mathcal{O}(\varepsilon^2)$ prediction of the theory. Similar analyses at different (x, t) values (not shown) also recovered this fact.

In these comparisons, $\alpha = 1/3$ was used. This represents a situation in which the interface was separated somewhat from the main channel boundary. If α were close to 0 or 1, the streamwise parabolic velocity profile (10) would have very rapid change in the y-direction, and consequently the y-excursions of the upstream streakline will be impacted by streamwise

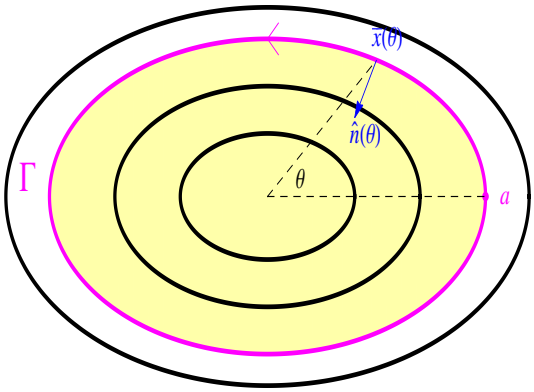

Figure 9. *Kirchhoff's elliptic vortex with a different fluid inside the streakline* Γ *[magenta].*

velocities which can be quite different from U. This can be quantified by the velocity shear at $y = 0$ in (10), which has size $(U/W)(1-2\alpha)/(\alpha-\alpha^2)$. An illustration of how the theoretical approximation breaks down in the high-shear (interface very near the boundary) instance is shown in Fig. 8. The blue curve is the theoretical streakline (with parameter values identical to the final panel in Fig. 6), and the red, orange and brown curves correspond to simulations with $\alpha = 0.1$, 0.06 and 0.04 respectively. The last of these values corresponds to a shear of approximately $24U/W$; the coefficient is very large. The tilt of the streaklines in this large shear situation cannot be captured by the theoretical approximation.

3.2. Anomalous fluid in a vortex. For this example, the attitude adopted by Turner [60] (see also [33, 67]) of modeling the interaction of a coherent vortex with its surroundings (consisting possibly of many other vortices distant to it, and also the effect of boundaries) by using a weak external strain field is adopted. While it would be convenient to use a line or Gaussian vortex with circular streamlines (on which particles flow at a constant speed) as the base flow, the utility of the method will be illustrated by using the more complicated Kirchhoff's classical elliptic vortex [32, 61, 41, 26, 39] as the prototype. In nondimensional coordinates in 2D, this has the flow given by

$$\left.\begin{aligned} \dot{x} &= -2y/m^2 \\ \dot{y} &= 2x/l^2 \end{aligned}\right\}, \tag{14}$$

with $m, l > 0$, which consists of nested elliptical streamlines centered at the origin. Suppose there are two different fluids inside and outside the elliptic streamline Γ defined by

$$\frac{x^2}{l^2} + \frac{y^2}{m^2} = 1\,,$$

as shown in Fig. 9, and take $\boldsymbol{a} = (l, 0)$. Another rationalization for the choice of this particular streamline could be that it is associated with a critical angular momentum value as dictated by an outer flow [60], thereby defining the 'boundary' of the vortex; however, the 'two-fluid'

paradigm as illustrated in Fig. 9 will be the main motivation which drives the analysis to follow. Before introducing an external strain field as an unsteady velocity agitation, a useful parametrization shall be presented. If θ is the standard polar angle, then the ellipse has a parametrization $\bar{\boldsymbol{x}}(\theta) = (\bar{x}, \bar{y}) = (l\cos\theta, m\sin\theta)$ with $\theta = 0$ being $\boldsymbol{a}$. So θ will be used instead of p to identify location/particle along the streakline. Therefore

$$|\boldsymbol{u}(\bar{\boldsymbol{x}}(\theta)| = \sqrt{\frac{4\bar{y}^2}{m^4} + \frac{4\bar{x}^2}{l^4}} = \frac{2}{ml}\sqrt{l^2\sin^2\theta + m^2\cos^2\theta}\,.$$

The rotation is anticlockwise around Γ, and thus the relevant normal unit vector is

$$\hat{\boldsymbol{n}}(\theta) := \frac{J\boldsymbol{u}\left(\bar{\boldsymbol{x}}(\theta)\right)}{|\boldsymbol{u}(\bar{\boldsymbol{x}}(\theta)|} = \frac{-1}{\sqrt{l^2\sin^2\theta + m^2\cos^2\theta}}\begin{pmatrix} m\cos\theta \\ l\sin\theta \end{pmatrix}$$

which points inwards as shown in Fig. 9. If τ is the time variation as a particle traverses Γ, then

$$|\boldsymbol{u}(\bar{\boldsymbol{x}}(\theta)|\,\mathrm{d}\tau = \sqrt{\bar{x}'(\theta)^2 + \bar{y}'(\theta)^2}\,\mathrm{d}\theta\,,$$

which leads to the relationship between the time τ and the polar location

$$\tau = \frac{ml}{2}\theta\,, \tag{15}$$

when the choice $\tau = 0$ when $\theta = 0$ (i.e., at $\boldsymbol{a}$) has been made.

Now, following a commonly modeled idea [48, 31, 24, 40, 35, 43, 60, 17, 67], suppose the vortex is placed in an unsteady strain field. Here, this is modeled by the inclusion of a weak unsteady velocity agitation $\boldsymbol{v}$ added to (14), subject to the constraint that $\boldsymbol{v}(\boldsymbol{a}, t) = \boldsymbol{0}$ for all t. Then, Theorem 1 gives the fact that the unsteady streakline at a location θ and time t perturbs in the direction $\hat{\boldsymbol{n}}(\theta)$ by an amount $M_v^{\mathrm{u}}(\theta, t)/\left|\boldsymbol{u}\left(\bar{\boldsymbol{x}}(\theta)\right)\right|$ (see also Fig. 9). The v subscript used here is for '*v*ortex,' to distinguish M^{u} from that of the previous example. Thus, the x- and y-coordinates of the unsteady streakline to leading-order obey

$$x_\varepsilon^{\mathrm{u}}(\theta, t) = l\cos\theta\left[1 - \frac{M_v^{\mathrm{u}}(\theta, t)m^2}{2\left(l^2\sin^2\theta + m^2\cos^2\theta\right)}\right] \tag{16}$$

and

$$y_\varepsilon^{\mathrm{u}}(\theta, t) = m\sin\theta\left[1 - \frac{M_v^{\mathrm{u}}(\theta, t)l^2}{2\left(l^2\sin^2\theta + m^2\cos^2\theta\right)}\right]. \tag{17}$$

The value of $M_v^{\mathrm{u}}(\theta, t)$ can be obtained from (8), with p now identified with θ, and by recasting the integral with respect to the polar angle as opposed to τ using (15):

$$M_v^{\mathrm{u}}(\theta, t) = -\int_0^\theta (m\cos\alpha, l\sin\alpha)\cdot\boldsymbol{v}\left(l\cos\alpha, m\sin\alpha, t + \frac{ml}{2}(\alpha - \theta)\right)\mathrm{d}\alpha\,. \tag{18}$$

The incompressibility of the flow means that the exponential term does not appear in the integral.

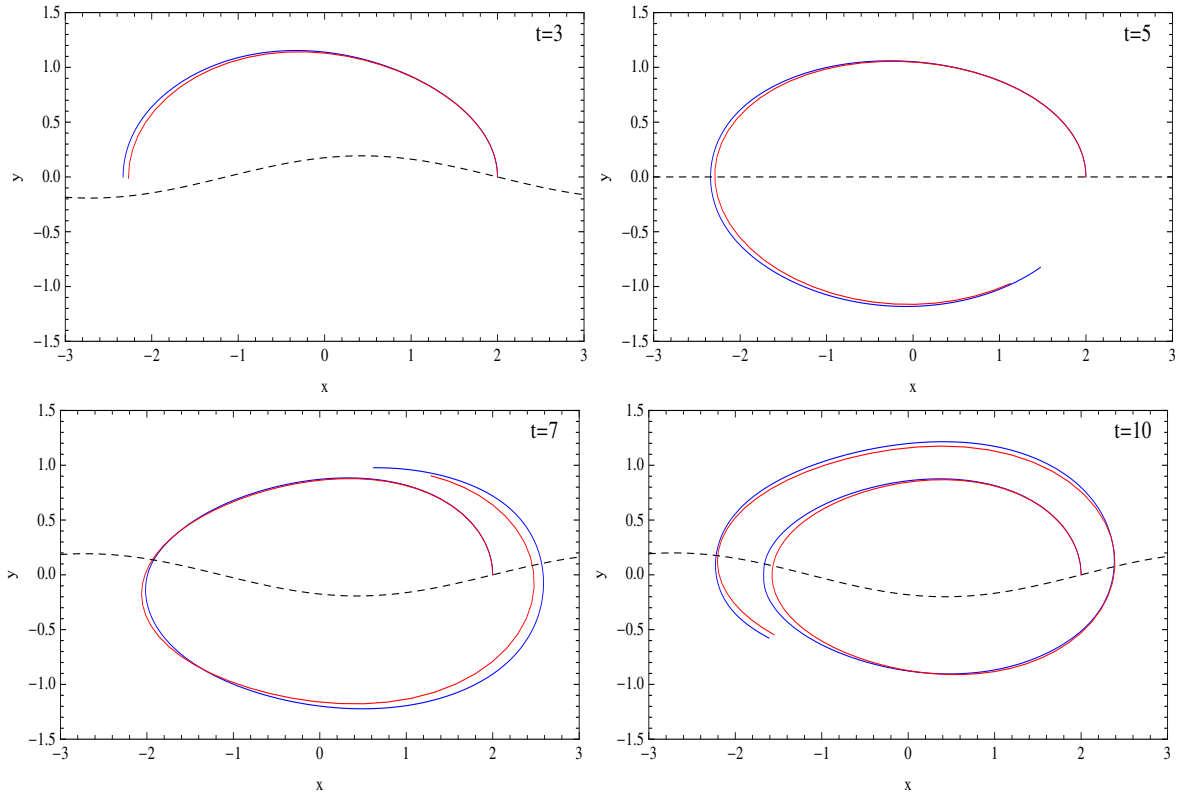

Figure 10. *Evolution of streakline [red], with dye released on the fluid interface at* $(2,0)$ *from time* 0 *onwards, and with the instantaneous velocity agitation (19)'s y-component variation shown by the black dashed curves. The blue curves are the theoretical approximation computed using (16), (17) and (18).*

Next, the theoretical flow interface, as characterized by the unsteady streakline expression above, shall be verified for a particular choice of unsteady velocity agitation $\boldsymbol{v}$. Suppose that, conforming with $\boldsymbol{v}(\boldsymbol{a},t)=\boldsymbol{0}$ for all t,

$$\boldsymbol{v}(x,y,t)=\varepsilon\sin(x-l)\begin{pmatrix}0\\1\end{pmatrix}\tanh(t-5) \tag{19}$$

is chosen, where $|\varepsilon|$ is small. This represents an agitation in the y-direction which is modulated periodically in x, but *aperiodically* in time. Thus, the expressions in (16) and (17) will be the expressions for the streakline, with error $\mathcal{O}(\varepsilon^2)$. The general expression (18) becomes in this situation

$$M_v^{\mathrm{u}}(\theta,t)=-\varepsilon l\int_0^\theta \sin\alpha\sin\left[l(\cos\alpha-1)\right]\tanh\left[t+\frac{ml}{2}(\alpha-\theta)\right]\,\mathrm{d}\alpha\,. \tag{20}$$

Numerical simulations of the streakline passing through $(l,0)$ are shown in red in Fig. 10 at different times, where $l=2$ and $m=1$, with red dye is released from time 0 onwards. To accentuate the variation displayed, the relatively large value of $\varepsilon=0.2$ is used. It should

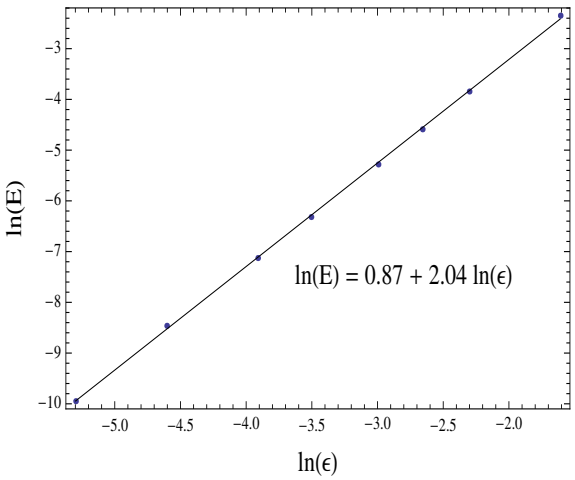

Figure 11. *The variation of the error between the numerically simulated and the explicit approximation (at $\theta = \pi$ and $t = 10$) with ε [dots] for the elliptic vortex, in a log-log plot.*

be noted that as t increases, the streaklines shown are not simple retracings and extensions of previous curves; the previous curves are themselves moving. The velocity agitation (19) considered here is purely in the y-direction, and displays a transition at $t = 5$ between two (almost) stationary states; this is displayed by the black dashed curve (scaled in the y-direction to be visible in this plot). A movie of the streakline evolution is provided with the Supplementary Materials. As the streakline wraps around, in this case the inner parts of the streakline accummulate towards an almost elliptic trajectory. The analytical expressions given by (16), (17) and (18) are used to generate the blue curves in Fig. 10. The agreement between the theoretical and numerical streaklines is good even at this value of ε. However, as the streakline wraps around, the analytical expression will be less accurate due to accumulation of errors. The matching between the curves when restricted to wrapping around just once is very good, and smaller ε values (not pictured), have greater accuracy (even for many wraps around). As shall be seen in Section 4, restricting to wrapping around less than once is sufficient *in evaluating transport of fluid.*

In analyzing the order of accuracy of the theoretical expression, the difference between the locations of the theoretical and numerical streaklines at the location $\theta = \pi$ and at the final time pictured in Fig. 10 was evaluated for many values of ε. The variation of the error with respect to ε is shown in a log-log plot in Fig. 11. The theoretically predicted accuracy of $\mathcal{O}(\varepsilon^2)$ is confirmed by this data. This same analysis (not shown) was performed at several different choices of gate location and time.

4. Transport quantification. Previous sections outlined theory and examples in determining streaklines under velocity agitations. Before the agitation, the flow interface between the two fluids was well-defined, with no transport occurring between the two fluids. The issue now is to quantify the intermingling between the two fluids after the agitation. Using a purely Lagrangian entity—the evolving flow interface as given by the streakline—across which transport is to be assessed does not work since the transport across this material curve

is zero. Similarly, using a purely Eulerian entity—the fixed flow interface in the absence of agitation—is inadequate since it fails to account for the evolving flow interface between the fluids, as discussed in Fig. 2.

The difficulties here are familiar in a different situation: when the interface consisted of a coincident stable and unstable manifold (a so-called heteroclinic manifold) before perturbation. After the agitation, it would split into stable and unstable manifolds which are not coincident, and which moreover move with time. In this case, the concept of lobe dynamics [48, 64] can be applied when the agitation is time-periodic in a specific way, or for more general perturbations it is possible to define an instantaneous transport [13, 7, 12], by adopting the idea of a gate as introduced by Poje and Haller [46]. While the current original flow interface is *not* a heteroclinic manifold, the ideas from [7, 12, 13] can be adapted to this situation.

Before perturbation, the flow interface was unequivocally defined by Γ, as shown in Fig. 3 for the open $\tilde{\Gamma}$ situation. This is the separating curve between the fixed regions R_1 and R_2, which were respectively occupied by fluids 1 and 2. Now, when the velocity agitation is included, at each time t there will be an unsteady streakline going through $\boldsymbol{a}$, shown in red in Fig. 12(a). This has the property that fluid on its two sides arrived from R_1 and R_2 respectively, and thus is identifiable as fluid 1 or 2. On the other hand, the streakline passing through $\boldsymbol{b}$ in the downstream direction (thick green curve) separates fluids which will eventually end up in the regions R_1 and R_2. There is potential for interchange of fluids because the unsteady streakline passing through $\boldsymbol{a}$ does not necessarily connect up with $\boldsymbol{b}$. To characterize this, draw a gate $\mathcal{G}(t)$ at the location $\boldsymbol{b}$ on Γ, by drawing a line which is locally perpendicular to Γ at $\boldsymbol{b}$. Shown in blue in Fig. 12(a), this is a line in the direction $\hat{\boldsymbol{n}}(p^{\mathrm{d}})$. The unit normal vector $\hat{\boldsymbol{g}}$ to $\mathcal{G}(t)$ shall be chosen to be

$$\hat{\boldsymbol{g}} := -J\,\frac{\boldsymbol{x}_\varepsilon^{\mathrm{u}}\left(p^{\mathrm{d}},t\right)-\boldsymbol{b}}{\left|\boldsymbol{x}_\varepsilon^{\mathrm{u}}\left(p^{\mathrm{d}},t\right)-\boldsymbol{b}\right|}\,. \tag{21}$$

i.e., this defines the orientation direction of the gate. Now the *nominal interface* $\Gamma_\varepsilon(t)$ at time t will be defined to be the union of the three connected curves (i) the streakline through $\boldsymbol{a}$ from upstream of $\boldsymbol{a}$ all the way up to the point $\boldsymbol{x}_\varepsilon^{\mathrm{u}}\left(p^{\mathrm{d}},t\right)$, (ii) the gate $\mathcal{G}(t)$ from $\boldsymbol{x}_\varepsilon^{\mathrm{u}}\left(p^{\mathrm{d}},t\right)$ to $\boldsymbol{b}$, and (iii) the forward-time streakline continuing on from $\boldsymbol{b}$. This is the collection of solid curves shown respectively in the colors red, blue and green in Fig. 12(a), which for emphasis is shown by the magenta curve in Fig. 12(b). Now, the backward-time streakline through $\boldsymbol{a}$, and the forward-time streakline through $\boldsymbol{b}$ remain unperturbed due to the velocity agitation. Therefore, the nominal interface retains the property the steady interface had: it separates space into two regions. In this case, because of the fact that the nominal interface is not identical to $\tilde{\Gamma}$ between $\boldsymbol{a}$ and $\boldsymbol{b}$, the spatial regions are no longer R_1 and R_2. Instead, they are regions $R_1(t)$ and $R_2(t)$ as indicated in Fig. 12(b). Both of these, and the nominal interface which separates them, are moving with time. Moreover, the nominal interface consists of two Lagrangian entities (the streakline segments) connected together by an quasi-Eulerian entity (the gate which is fixed in time, but whose upper limit $\boldsymbol{x}_\varepsilon^{\mathrm{u}}\left(p^{\mathrm{d}},t\right)$ is affected by the Lagrangian flow), and is therefore a hybrid entity.

The *flux* is now defined to be the instantaneous fluid flux from the region $R_2(t)$ to $R_1(t)$, where the 1 and 2 are chosen such that the vector $\hat{\boldsymbol{n}}(p^{\mathrm{d}})$ points from $R_2(t)$ to $R_1(t)$. Since the boundary between these regions, the nominal interface $\Gamma_\varepsilon(t)$, is *evolving with time*, flux needs

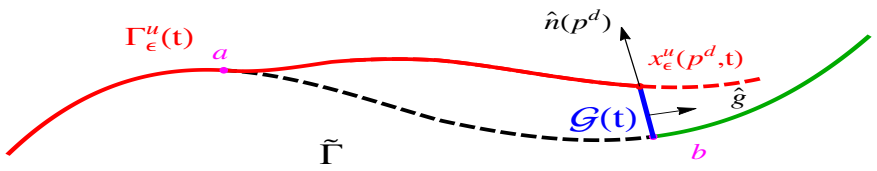

(a) Streakline (red) and gate (blue)

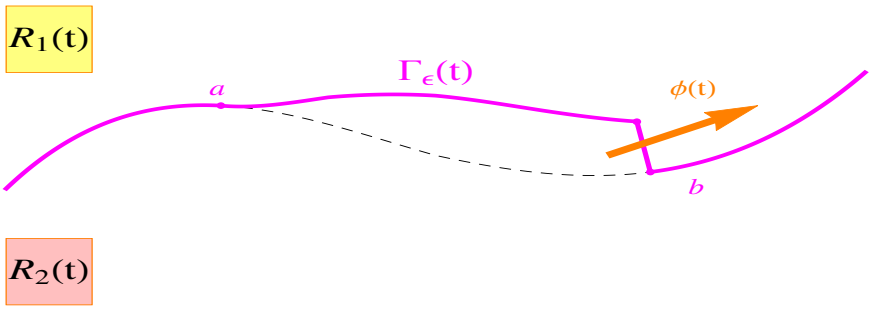

(b) Nominal streakline (magenta)

Figure 12. *Construction of the nominal interface for transport assessment, from the configuration in Fig. 4.*

to be measured relative to this. The streakline segments of $\Gamma_\varepsilon(t)$ are Lagrangian entities, and therefore there is *no* flux across them[3]. The flux from $R_2(t)$ to $R_1(t)$ is therefore simply the flux across the gate, and is given by

$$\phi(t) = \int_{\mathcal{G}(t)} \left[\boldsymbol{u}\left(\boldsymbol{x}(\ell)\right) + \boldsymbol{v}\left(\boldsymbol{x}(\ell), t\right)\right] \cdot \hat{\boldsymbol{g}}\, \mathrm{d}\ell\,, \tag{22}$$

in which $\boldsymbol{x}(\ell)$ is a parametrization along $\mathcal{G}(t)$ with respect to arclength ℓ. The ϕ above is explicitly a flux in the sense that it is an area of fluid per unit time which crosses the nominal interface instantaneously. Moreover, there is a sign convention for $\phi(t)$. In the situation pictured in Fig. 12(b), fluid 2 crosses $\Gamma_\varepsilon(t)$ from $R_2(t)$ to $R_1(t)$, that is, in the direction associated with $\hat{\boldsymbol{n}}(p^{\mathrm{d}})$ in relation to the original Γ. This occurs since the streakline in Fig. 12(a) is above the point $\boldsymbol{b}$ at the gate location. In other words, the unit vector $\hat{\boldsymbol{n}}(p^{\mathrm{d}})$ is in the same direction as $\boldsymbol{x}^{\mathrm{u}}_\varepsilon\left(p^{\mathrm{d}}, t\right) - \boldsymbol{b}$. If the streakline were below $\boldsymbol{b}$, then the picture corresponding to Fig. 12(b) would have a flux of fluid 1 from region $R_1(t)$ to $R_2(t)$. However, dominant flow direction across the gate would still be from left to right, but now the vectors $\hat{\boldsymbol{n}}(p^{\mathrm{d}})$ and $\boldsymbol{x}^{\mathrm{u}}_\varepsilon\left(p^{\mathrm{d}}, t\right) - \boldsymbol{b}$ would be in opposite directions. This results in $\hat{\boldsymbol{g}}$ pointing in the

[3]There may be normal velocities across these, but this causes the streaklines themselves to move in the normal direction.

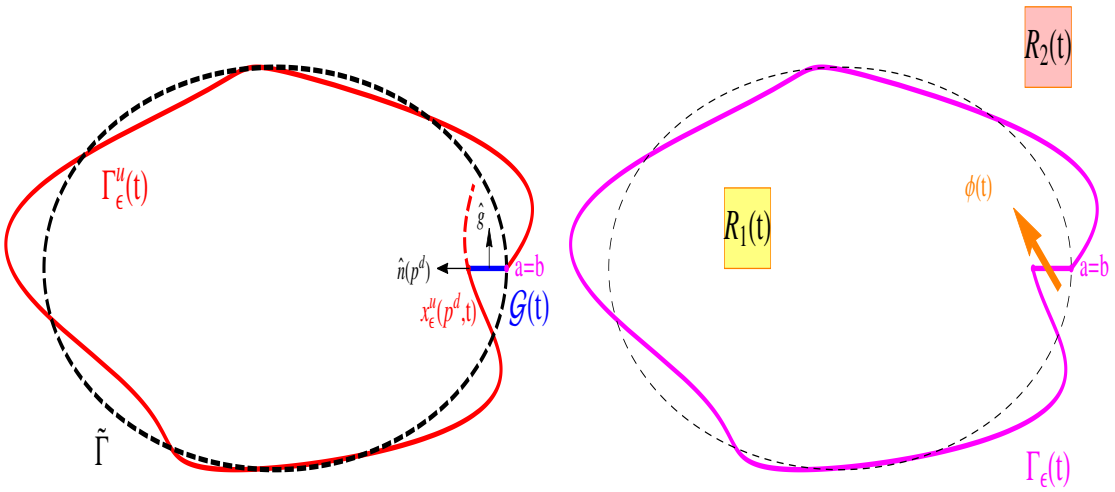

(a) Streaklines and gate (b) Nominal streakline (magenta)

Figure 13. *Construction of the nominal interface for closed* $\tilde{\Gamma}$.

opposite direction to that shown in Fig. 12(a), i.e., to the left. The flux, then, from (22) would be negative. Thus, the convention is that $\phi(t) > 0$ if the flux is from $R_2(t)$ to $R_1(t)$, and negative if in the opposite direction.

At instances in which $\boldsymbol{x}^{\mathrm{u}}_{\varepsilon}\left(p^{\mathrm{d}}, t\right) = \boldsymbol{b}$, $\hat{\boldsymbol{g}}$ would be undefined, but in this case the gate has zero size, and so the flux is instantaneously zero. As time progresses, the quantity $\phi(t)$ could keep changing sign, resulting in flux going to and fro between $R_1(t)$ and $R_2(t)$.

The interpretation of the nominal interface and flux for *closed* $\tilde{\Gamma}$ is particularly illuminating. Since in this case $\boldsymbol{a} = \boldsymbol{b}$, think of glueing $\boldsymbol{a}$ to $\boldsymbol{b}$ in Fig. 12, and throwing away the parts upstream of $\boldsymbol{a}$ and downstream of $\boldsymbol{b}$. The resulting picture is shown in Fig. 13, and it is clear here that the third component which defines $\Gamma_\varepsilon(t)$ (the green streakline going beyond $\boldsymbol{b}$ as shown in Fig. 12(a)) does not apply here. The two regions $R_1(t)$ and $R_2(t)$ in this case are interior and exterior regions, separated by $\Gamma_\varepsilon(t)$. Thus, (22) quantifies the transfer of fluid from the outside to the inside region. At the instance pictured, $\phi(t) > 0$, corresponding to a transport of fluid 2 into $R_1(t)$. Another way of saying this is that $\phi(t)$ represents the rate of change of the area of the interior region $R_1(t)$, whose boundary is the nominal interface $\Gamma_\varepsilon(t)$.

This method allows for easy representation of $\phi(t)$'s variation with time. This is different from approaches which—in various settings—attempt to capture the transfer of fluid over a certain time period [42, 30]. Knowing the time-variation gives more information than simply knowing the amount of fluid transferred over a fixed time. For example, consider a situation in which $\phi(p, t)$ flips sign repeatedly during a time-interval in which it is necessary to understand transport. This would imply that small amounts of fluid of one type are injected into regions dominated by the other type (and vice versa). In contrast, if $\phi(t)$ changed sign just *once* during

the time-interval but was associated with the same amount of fluid, this would indicate that one *large* blob of each fluid type has gone into a region dominated by the other. The area of the transferred fluids may be the same in these two different scenarios, but in the former (many small amounts of fluids) situation there will be considerably more mixing between the fluids. This is because the smaller scales will subsequently be more affected by diffusion, and the displaced fluid blobs will therefore homogenize quicker into the surrounding fluid than in the case of the larger blob. Thus, having a method which enables quick knowledge of ϕ's time-variation allows for judging the resulting mixing properties between the fluids.

Had one simpy wanted to know the *amount* of fluid transferred during a particular time-period, this is of course easily obtainable from $\phi(t)$. The amount of fluid 2 transported from $R_2(t)$ to $R_1(t)$ over time $t \in [T_i, T_f]$ would be

$$\Phi_{2\to 1} = \int_{T_i}^{T_f} \phi(t)^+ \,\mathrm{d}t\,, \tag{23}$$

where ϕ^+ is the positive part of ϕ (that is, $\phi^+ = \phi$ when $\phi \geq 0$, but $\phi^+ = 0$ when $\phi < 0$). The opposite flow of fluid 1 from $R_1(t)$ to $R_2(t)$, $\Phi_{1\to 2}$, could similarly be defined.Thus, knowing the time-variation of ϕ gives a range of information on the transport process.

While the nominal interface and flux definitions work for general velocity fields, it is not clear whether the flux would be easily computable. In the present context in which the velocity is dominantly steady, however, a leading-order expression for ϕ is possible:

Theorem 2 (Instantaneous transport). *The instantaneous flux $\phi(t)$ across the nominal interface is*

$$\phi(t) = M(t) + \mathcal{O}(\varepsilon^2) \tag{24}$$

where

$$M(t) := \int_{p^{\mathrm{u}}}^{p^{\mathrm{d}}} \exp\left[\int_{\tau}^{p^{\mathrm{d}}} \left[\boldsymbol{\nabla}\cdot\boldsymbol{u}\right](\bar{\boldsymbol{x}}(\xi))\,\mathrm{d}\xi\right] \left[J\boldsymbol{u}\left(\bar{\boldsymbol{x}}(\tau)\right)\right]\cdot\boldsymbol{v}\left(\bar{\boldsymbol{x}}(\tau), \tau + t - p^{\mathrm{d}}\right)\mathrm{d}\tau\,. \tag{25}$$

For the proof, the reader is referred to Appendix B. The power of Theorem 2 is that, unlike in the definition (22), the instantaneous flux can be represented in terms of known quantities from the steady flow, and the unsteady velocity. Unsteady *trajectories* (and in particular the unsteady streaklines) are not needed.

A question that may be posed is whether slicing off the streakline on the gate in creating the nominal interface loses information. After all, the continuation of the streakline could potentially be highly complicated. The construction of the nominal interface, however, *does* take all this information into account, in the following way. All points which lie on a streakline will at an appropriate time instance pass through the gate. Therefore, the missing information at a particular time instance (i.e., the dashed portions of the streaklines whose beginnings are shown in Figs. 12(a) and 13(a)) will become incorporated into the nominal streakline at some other instance in time. In other words, the time-variation of ϕ will encode this information. So, for example, even if the continuations of the streaklines in Fig. 13(a) wrap around many times within the closed region, knowing the streaklines up to the point at which they intersect

the gate is sufficient for the transport quantification. The nominal interface construction provides a method for simplifying the potentially highly complicated intersection patterns between the streaklines to obtain a transport measure.

Is (24) equivalent to an Eulerian flux definition under some conditions? Under the condition of fluid incompressibility, $\boldsymbol{\nabla} \cdot \boldsymbol{u} = 0$, and (25) becomes

$$M(t) := \int_{p^{\mathrm{u}}}^{p^{\mathrm{d}}} \left[J\boldsymbol{u}\left(\bar{\boldsymbol{x}}(\tau)\right)\right] \cdot \boldsymbol{v}\left(\bar{\boldsymbol{x}}(\tau), \tau + t - p^{\mathrm{d}}\right) \mathrm{d}\tau \,. \tag{26}$$

Now, the Eulerian flux across $\tilde{\Gamma}$ at an instance t in time is given by

$$E(t) = \int_{\tilde{\Gamma}} \frac{J\boldsymbol{u}\left(\bar{\boldsymbol{x}}\right)}{\left|\boldsymbol{u}\left(\bar{\boldsymbol{x}}\right)\right|} \cdot \boldsymbol{v}\left(\bar{\boldsymbol{x}}, t\right) \mathrm{d}\ell$$

where $\bar{\boldsymbol{x}}$ represents positions on $\tilde{\Gamma}$ and ℓ is the arclength parametrization. By parametrizing with respect to τ according to $\left|\boldsymbol{u}\left(\bar{\boldsymbol{x}}(\tau)\right)\right| = d\ell$, this can be rewritten as

$$E(t) = \int_{p^{\mathrm{u}}}^{p^{\mathrm{d}}} \left[J\boldsymbol{u}\left(\bar{\boldsymbol{x}}(\tau)\right)\right] \cdot \boldsymbol{v}\left(\bar{\boldsymbol{x}}(\tau), t\right) \mathrm{d}\tau \,, \tag{27}$$

which is equivalent to (26) only if $\boldsymbol{v}$ is steady. If incompressibility *and* steadiness are not *both* satisfied, the flux defined here is therefore different from a simple Eulerian flux. In comparing (26) and (27) for example, $\boldsymbol{v}$ is evaluated at a retarded time in the former in comparison to the latter. This accounts for the antecedents of a fluid particle; it is not just the current location which matters, but where it came from.

The transport definition developed here has connections to a recent article by Karrasch [30]. In terms of the present setting, this partitions space at time 0 according to the number of times trajectories beginning in the sets cross a time-varying curve over a time-interval $[0, T]$. This is related to the integrated net flux (defined in extended state space) across this curve during this time. If the time-variation of the nominal interface is viewed as Karrasch's time-varying curve, along the parts composed on streakline segments: (i) there is no flux, and (ii) no trajectories cross. There are contributions to both these only in the segments composed of the gate. Moreover, Karrasch uses a streakline idea as the interaction between Eulerian and Lagrangian coordinates; this is similar in spirit to using the streakline here to map back upstream [30]. However, the present paper differs in that it obtains a *time-varying* as opposed to a time-integrated flux definition, and moreover constructs the relevant time-varying curve (the nominal interface) as arising from the flow due to the presence of two fluids, as opposed to specifying it.

5. Transport validation.

The two examples examined in Section 3 are now re-examined. Here, the focus is on determining the advective flux as a result of the moving streaklines.

5.1. Two fluids in a microchannel.

Consider two fluids in a microchannel, with exactly the velocity agitation and parameter values as used in Section 3. Here, $\boldsymbol{b}$ is any point beyond the final cross-channel, and so $\boldsymbol{b} = (5.5, 0)$ (corresponding to $p^{\mathrm{d}} = 5.5/U$) is chosen. To numerically simulate the upstream streakline at some instance in time t, it is therefore necessary

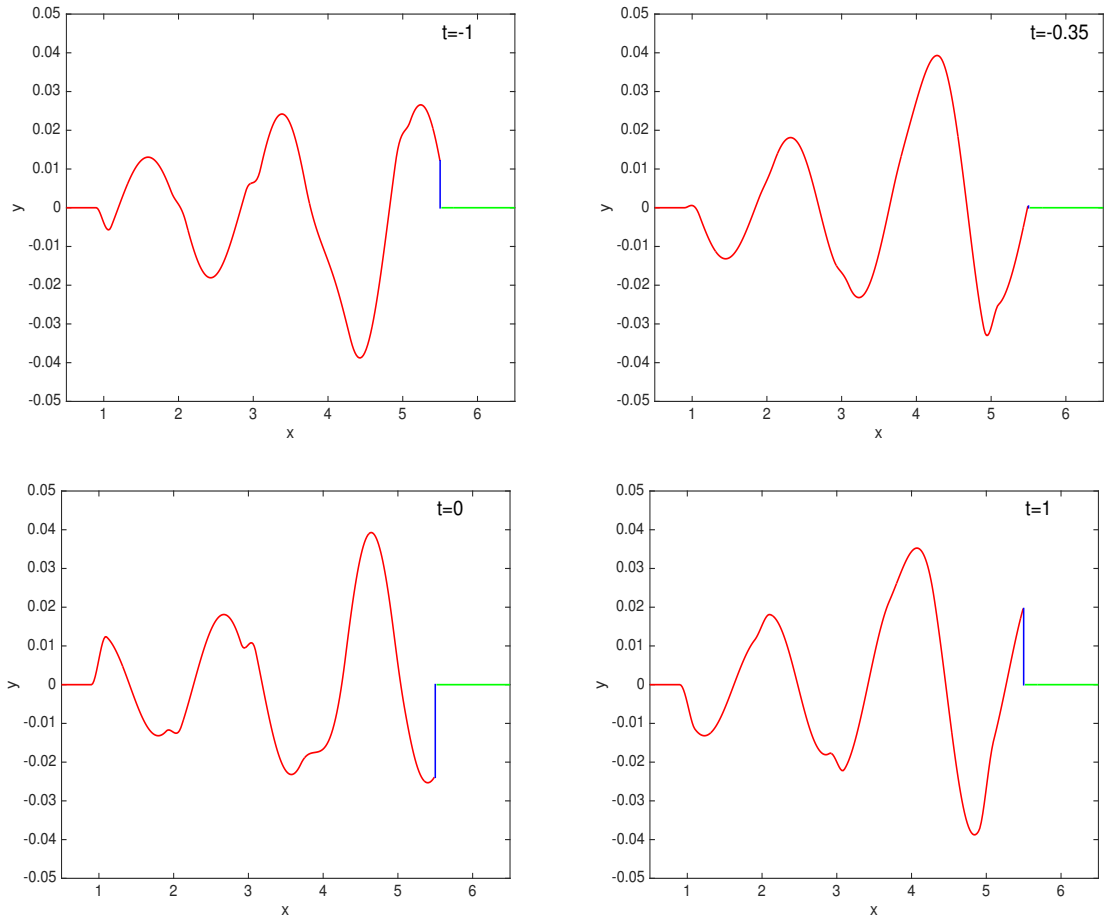

Figure 14. *Nominal interfaces for the channel flow obtained by numerical simulation, at several instances in time. The color-coding of the nominal interfaces is consistent with Fig. 12(a), showing the upstream streakline [red], gate [blue] and downstream streakline [green].*

to release particles from $\boldsymbol{a} = (0.5, 0)$ at times prior to t, and allow the streakline to evolve until it intersects a vertical line drawn at $x = 5.5$. An overestimate for the time needed is used, the streaklines are numerically evaluated at the desired time t, and then parts of the streakline which have overshot the gate are excised. The downstream streakline beyond $\boldsymbol{b}$ in this case simply lies along the x-axis. Fig. 14 shows the nominal interfaces obtained by this process at four different times. At $t = -1$, the flow direction through the gate is such that fluid will get transported from $R_2(-1)$ to $R_1(-1)$. Since in the direction of $\hat{\boldsymbol{n}}$, this represents a positive instantaneous flux. At $t = 0$, the flux is negative, and this indicates the presence of at least one value between -1 and 0 at which the instantaneous flux is zero. Bisection was used to determine a value of approximately $t = -0.35$ (shown in the second panel of Fig. 14), at which instance the red streakline essentially hits $\boldsymbol{b}$, resulting in the gate having zero length. At the later time $t = 1$, the flow is once again from $R_2(t)$ to $R_1(t)$. As time

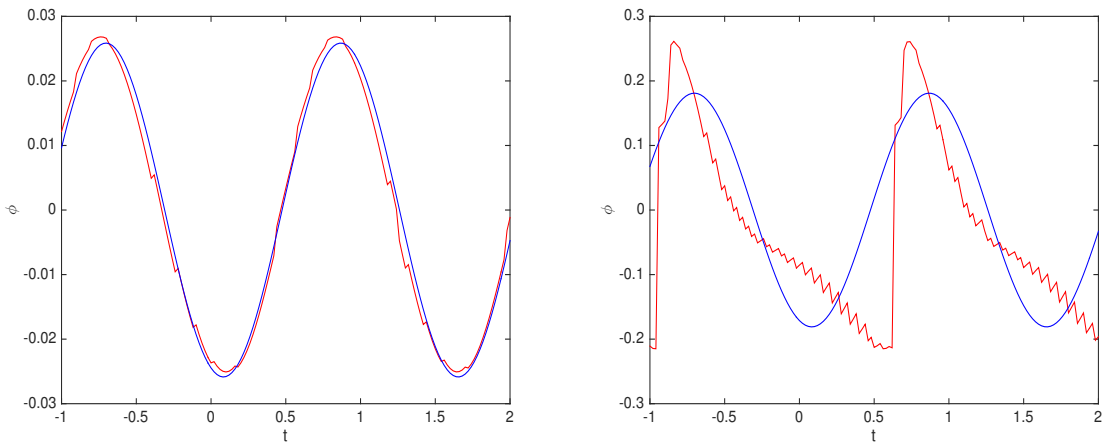

(a) $\varepsilon = 0.1$ (b) $\varepsilon = 0.7$

Figure 15. *Transport from $R_2(t)$ to $R_1(t)$ in the channel using numerical simulation [red] and the analytical expression (28) [blue], for the agitation and parameter values as specified in Section 3.*

progresses, repeated interchanges of relative positioning along the gate occurs, implying that fluid sloshes to and fro across the nominal interface $\Gamma_\varepsilon(t)$, causing an advective interchange of fluids between regions $R_1(t)$ and $R_2(t)$.

Next, the flux shall be compared to the analytical expression in Theorem 2. Before writing the instantaneous flux expression for this specific configuration, it can be written for a *general* channel configuration as described in Section 3 by

(28)
$$M_c(t) = \int_{p_1-d_1/U}^{p_n+d_n/U} \sum_{j=1}^{n} \mathbb{I}_{[p_j-d_j/U,p_j+d_j/U]}(\tau) U \frac{v_j}{d_j^2} \left[U^2\,(\tau-p_j)^2 - d_j^2\right] \cos\left[\omega\left(\tau+t-p^{\mathrm{d}}\right)+\phi_j\right] \mathrm{d}\tau\,,$$

where $\mathbb{I}$ is the indicator function. It is clear that the flux is periodic in t with period $2\pi/\omega$, and is explicitly calculable for given parameter values. Now, for the specific channel configuration and parameter values as examined in Section 3, the analytical expression is compared with that obtained by simulations results inserted into the flux definition (22) in Fig. 15. In (a), the particular value $\varepsilon = 0.1$ of Section 3 has been used, with the red curve generated from the numerics, while the blue curve is the analytical approximation. Numerically determining the flux at a time t requires several steps. First, fluid particles were synthetically released from $\boldsymbol{a}$ during a time interval $[t_-, t]$, with t_- chosen to ensure that by time t, the upstream streakline would have gone beyond the gate. This enables the determination of the intersection point between the upstream streakline and the gate at time t, and allows for (22) to be used to compute the flux across the gate by integration. This procedure was followed for each t shown in Fig. 15(a). In spite of the fact that the perturbative theoretical flux essentially treats this normal velocity as a constant along the gate, the curves are very close. In (b), the comparison is performed with $\varepsilon = 0.7$ (but everything else kept identical), showing that indeed the theory loses predictive ability when the agitation is comparable to the main flow. Having

said that, the theoretical blue curve, obtained using perturbative methods in ε, provides good information on the dominant behavior of the flux.

5.2. Anomalous fluid in a vortex. Let us return to the elliptic votex flow. Unlike in the previous example, the flow on $\tilde{\Gamma}$ is not of a constant speed, $\tilde{\Gamma}$ is curved, and the velocity agitation is not always perpendicular to $\tilde{\Gamma}$. Determining the nominal interface at a general time t will therefore be more complicated. Take $\boldsymbol{a} = (l, 0)$ as before, and let $\boldsymbol{b}$ be the identical point but after the vortical flow has taken the particle released from $\boldsymbol{a}$ one round around the vortex. Thus, when using θ instead of p as a parameter, $\boldsymbol{a}$ corresponds to $\theta = 0$ and $\boldsymbol{b}$ to 2π. The gate drawn at $\boldsymbol{b}$ is on the x-axis, and so the transport depends on exactly one rotation of the streakline. This avoids having to deal with accumulated errors when streaklines wrap around more than once, as seen in Section 3. Furthermore, such further points of the streaklines will eventually pass through the gate, and thus by including the time-dependence of the transport function, the impact of the extended streaklines is included in this analysis.

Numerically determining the nominal interface at an instance in time t entails first releasing particles from $\boldsymbol{a}$ continually from some time instance in the past, and then allowing the streakline to evolve until it crosses the gate $\mathcal{G}(t)$ on the x-axis. Particle release is done at a time $1.2\pi ml$ prior to each required time t, from since in the absence of a velocity agitation the time of flow around Γ would be exactly πml from (15). This is an overestimate for the required time and, at time t, parts of the streakline which have extruded beyond $\mathcal{G}(t)$ are clipped. Using exactly the parameter values as in Section 3, the nominal interfaces were obtained using this procedure at different times t, and are pictured in Fig. 16 by the solid curves. Given that the dominant flow is counter-clockwise, the instantaneous flux is going *out of* the vortex at all instances pictured, with a larger value at the intermediate times shown, and being very small at $t = 4$ and 12.

An insight for this behavior can be obtained from the theoretical approximation for the flux function. Since $\theta^{\mathrm{d}} = 2\pi$, the instantaneous flux function is

$$M_v(t) = -\int_0^{2\pi} (m\cos\alpha, l\sin\alpha)\cdot \boldsymbol{v}\left(l\cos\alpha, m\sin\alpha, t + \frac{ml}{2}(\alpha - 2\pi)\right)\,\mathrm{d}\alpha\,, \tag{29}$$

which for the specific velocity perturbation considered in Section 3 becomes

$$M_v(t) = -\varepsilon l\int_0^{2\pi} \sin\alpha\sin\left[l(\cos\alpha - 1)\right]\tanh\left[t - 5 + \frac{ml}{2}(\alpha - 2\pi)\right]\,\mathrm{d}\alpha\,. \tag{30}$$

This is shown by the blue curve in Fig. 17 for the same parameter values used for the numerical simulation. The red curve is that obtained by directly applying the flux formula (22) to the numerical simulations, that is, to computations of the gate à la Fig. 16 and integrating the normal velocity across the gate. Good agreement is obtained, bearing in mind the fact (30) uses only values *on* $\tilde{\Gamma}$, while the true flux calculation of (22) is impacted by the variation away from $\tilde{\Gamma}$. Both curves indicate that the flux is negative for all times, and thus fluid leaks from the inside to the outside of the vortex. This will be visible as a tendril or filament of the inner fluid escaping to the outer one, with the tendril wrapping around in the anti-clockwise direction. It is interesting that this new approach reveals exactly the qualitative behavior that is well-documented for vortices in external shear flows [40, 16, 17]. From the mixing perspective,

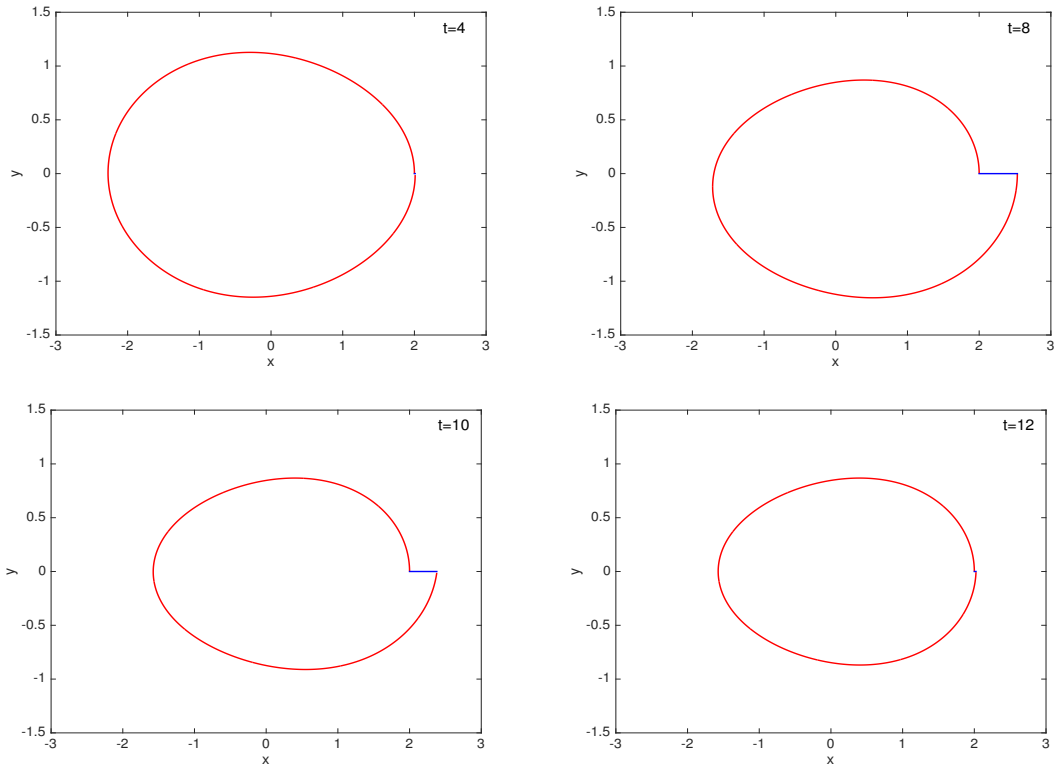

Figure 16. *Nominal interfaces for the agitated elliptic vortex flow obtained by numerical simulation, at several instances in time. The color-coding of the nominal interfaces is consistent with Fig. 13(a).*

diffusion would then act on the tendril, causing the inner fluid to become dispersed in the outer one. The effect of diffusion is not explicit in the theory here, which focusses specifically on the advective (Lagrangian) flow. However, in reality this advective process promotes fluid mixing through advection-driven diffusion. Smaller ε values [not shown] lead to even better agreement between the analytical approximation and the numerical flux.

A minor point which must be made is the connection to incompressibility, which is satisfied for the velocity conditions chosen in this example. Does the fact that there is a flux exiting the vortex for all time contradict incompressibility? The answer is no, since the closed nominal interface—the purported flow interface under unsteady conditions—compensates for the expelled fluid by shrinking in. This is indeed visible by comparing the areas enclosed within the closed nominal interfaces in Fig. 16; these get smaller as t increases. Indeed, when $\tilde{\Gamma}$ is closed, the rate of change of the area enclosed by the nominal interface is *precisely* the definition of the instantaneous flux.

6. Concluding remarks.

The concepts of stable and unstable manifolds—and various finite-time analogues often loosely referred to as Lagrangian Coherent Structure approaches [28, 13, 50]—are important in demarcating flow barriers in *single phase* unsteady flows. Here, the focus is on *two-phase* flows, in which such entities derived purely by examining the velocity

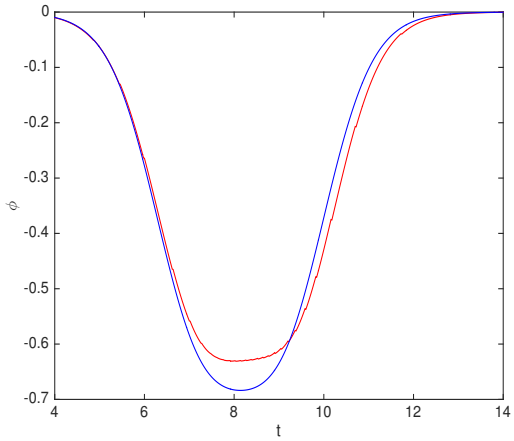

Figure 17. *Transport into the elliptic vortex using numerical simulation [red] and the analytical expression (29) [blue], for the agitation conditions and parameters as specified in Section 3.*

field do not distinguish the flow barrier. In the steady, as-yet-unmixed situation, the flow barrier is the *interface* between the two fluids, which is identified physically as opposed to from characteristics of the fluid velocity. This article has focussed on determining the flow interface, and rationalizing and quantifying the transport between the two fluids, when an unsteady velocity agitation is introduced. The relevance of streaklines has been highlighted, and their usage in defining a *nominal interface*, and quantifying an instantaneous transport across this has been elucidated. Under the condition that the velocity agitation is weak (i.e., has speeds significantly smaller than that of the base steady velocities), a theory for determining the streaklines, and the transport flux, has been developed. Validations of the method in comparison to numerically computed streaklines was performed for the open (two fluids flowing along a channel) and closed (a blob of one fluid inside a vortex) flow interfaces situations.

The method for quantifying the transport across the flow interface developed in this paper depends on the velocity agitation being small in comparison to the base flow, which is steady. However, this does *not* require incompressibility, nor a particular form of time-dependence. Indeed, it is likely that recent work [14] which characterizes the effect of an *impulsive* velocity (such as obtained by tapping a fluidic device, say) on stable/unstable manifolds, can be modified to determine the streaklines and transport associated with a non-heteroclinic flow interface, consonant for example with the impulsively strained vortex numerics of [17].

Optimizing fluid mixing is a topic which has elicited some recent interest [53, 29, 37, 23, 56, 54]. The presence of a theoretical approximation for the transport offers scope in being able to optimize transport in a specific sense: across the flow interface. Such has been done in the case where the flow barrier was a heteroclinic manifold (coincident stable and unstable manifold) in the situation where a sinusoidally varying velocity agitation was applied [6, 4, 15, 8]. Given that the transport expression (25) obtained in this non-heteroclinic instance shares some similarities with the heteroclinic theory of [6, 4, 15, 8], there is obvious

scope in being able to adapt those ideas to this situation. There is considerable evidence of the presence of an optimal frequency of a velocity agitation in order to maximize mixing [8, 36, 62, 52, 44]; would it be possible to determine this in, for example, configurations such as that of the channel examined here? Alternatively, can one obtain insight into the best positioning of cross-channels to effect the best mixing across the flow interface? Questions such as these are under investigation, and will be reported on in follow-up work.

The approach presented here offers a different viewpoint on the oft-examined vortex-in-an-external-strain problem [48, 31, 24, 40, 35, 43, 60, 17, 39, 26], in the sense that it permits a direct computation of the fluid flux into, or out of, the vortex as a function of time, for a given weak external strain field. In this sense, it captures Lagrangian transport, as opposed to standard methods which, for example, picture the time evolution of the frozen-time (Eulerian) vorticity field [17, 60]. There are of course connections between the Lagrangian and Eulerian viewpoints, but in cases where the *transport* is important, the current approach may provide new insights.

The closed flow interface situation appears to be of particular interest in modeling how a blob of fluid (an oil/pollutant/nutrient/plankton/chemical patch) which is placed in an anomalous fluid mixes in with its surroundings. Once again, 'standard' methods for detecting coherent structure boundaries directly from the velocity field are not necessarily applicable, since the flow interface is a physical boundary between two fluids as opposed to an entity derivable from the velocity field. The methods outlined in this article are a first step towards understanding the Lagrangian transport associated with this from a theoretical perspective. The trick is trying to identify the flow interface in the presence of an unsteady velocity, which can be done here if there is an anchor point on the interface at which the *unsteady* component of the velocity is zero. If not, there is a difficulty in deciding where to release particles for the streakline determination. How one might figure out the nominal interface (i.e., the relevant unsteady flow interface) when there is no such anchor point is not clear. Note that the process of evolving particles on the closed steady flow interface (i.e., examining the *timeline*) is not effective in assessing transport, since this closed loop simply remains a closed loop under unsteady velocity agitations, and therefore a transport between the interior and exterior *across this* is zero. This is of course true for any material curve, which precludes their usage for transport assessment. A nominal flow interface across which there is transport needs to be enunciated. The ability to do so using streaklines when there is at least one anchor point, as outlined here, can hopefully be build on, in the situation of weak strain which is never zero on the interface.

The methods described in this article offer another tool for analysis of transport, in this case *diffusive* transport. With pure advection, the streakline through $\boldsymbol{a}$ remains a separator between the two fluids. However, if diffusion is also taken into account [59, 11, 24, 40], then effective transport may occur if the streakline develops sufficient undulations and filamentations. The advantage of the explicit formulas developed in Section 2 for the streakline is that a measure of complexity (e.g., the total variation) can then be derived for the streakline. Given that the velocity agitation is embedded within the formula, this provides a new tool for analyzing, and possibly optimizing, the measure of complexity with respect to the velocity agitation. Further analysis of this is underway.

Appendix A. Proof of Theorem 1 [Upstream streakline].

The proof here is in the spirit of the proof of Theorem 2.1 in [9], in which an unstable manifold's displacement is characterized. However, this situation is different, since it is the *streakline* that is required. Imagine fixing the time t, and also the particle p in this time-slice which is at the location $\bar{\boldsymbol{x}}(p)$ in the steady flow (1). Due to the action of the unsteady velocity agitation $\boldsymbol{v}$, this particle will be at a nearby location, $\mathcal{O}(\varepsilon)$ away, at a location $\boldsymbol{x}^{\mathrm{u}}_{\varepsilon}(p,t)$. *Thinking of* (p,t) *as fixed*, but with τ as the time-variable, define

$$M^{\mathrm{u}}(p,\tau) = [J\boldsymbol{u}(\bar{\boldsymbol{x}}(\tau-t+p))] \cdot [\boldsymbol{x}^{\mathrm{u}}_{\varepsilon}(p,\tau) - \bar{\boldsymbol{x}}(\tau-t+p)] \,. \tag{31}$$

From (2), it is clear that $\bar{\boldsymbol{x}}(\tau - t + p) = \boldsymbol{x}^{\mathrm{u}}_0(p,\tau)$, the steady streakline at location p; this passed through $\boldsymbol{a}$ a time $p - p^{\mathrm{u}}$ prior to τ. For the *unsteady* flow streakline as defined through (5), $\boldsymbol{x}^{\mathrm{u}}_{\varepsilon}(p,\tau)$ represents the location of the same particle, and thus $\boldsymbol{x}^{\mathrm{u}}_{\varepsilon}(p,\tau) - \bar{\boldsymbol{x}}(\tau-t+p)$ is the difference occurring as the result of including $\boldsymbol{v}$. This difference is $\mathcal{O}(\varepsilon)$ since $\boldsymbol{v}$ is $\mathcal{O}(\varepsilon)$, and then so is $M^{\mathrm{u}}(p,\tau)$. Note moreover that

$$\frac{M^{\mathrm{u}}(p,t)}{|\boldsymbol{u}\left(\bar{\boldsymbol{x}}(p)\right)|} = \frac{J\boldsymbol{u}\left(\bar{\boldsymbol{x}}(p)\right)}{|\boldsymbol{u}\left(\bar{\boldsymbol{x}}(p)\right)|} \cdot [\boldsymbol{x}^{\mathrm{u}}_{\varepsilon}(p,t) - \bar{\boldsymbol{x}}(p)] \tag{32}$$

is the projection of the displacement of the streakline in the direction normal to Γ at $\bar{\boldsymbol{x}}(p)$. Hence, the goal is to determine $M^{\mathrm{u}}(p,t)$ in terms of known quantities from the steady flow. To do this, it is necessary to differentiate (31) with respect to τ at fixed (p,t). Fortunately, it turns out that this part of the calculation is *identical* to that in the proof of Theorem 2.1 in [9], and hence by inspection of equation (3.6) of [9] it is possible to write

$$\begin{aligned} &\frac{\partial M^{\mathrm{u}}}{\partial \tau} - \left[\boldsymbol{\nabla}\cdot\boldsymbol{u}\right]\left(\bar{\boldsymbol{x}}(\tau-t+p)\right) M^{\mathrm{u}} \\ &\qquad = \left[J\boldsymbol{u}\left(\bar{\boldsymbol{x}}(\tau-t+p)\right)\right] \cdot \boldsymbol{v}\left(\bar{\boldsymbol{x}}(\tau-t+p),\tau\right) \,, \end{aligned} \tag{33}$$

where $\mathcal{O}(\varepsilon^2)$ terms have been discarded. Next, (33) will be multiplied by the integrating factor

$$\mu(\tau) := \exp\left[-\int_0^{\tau} \left[\boldsymbol{\nabla}\cdot\boldsymbol{u}\right]\left(\bar{\boldsymbol{x}}(\xi-t+p)\right) \mathrm{d}\xi\right] \,,$$

and integrated from $\tau = t + p^{\mathrm{u}} - p$ to t. Before proceeding, the lower limit will require some explanation. When inserted into (31) this yields

$$\begin{aligned} M^{\mathrm{u}}(p, t+p^{\mathrm{u}}-p) &= [J\boldsymbol{u}(\bar{\boldsymbol{x}}(p^{\mathrm{u}}))] \cdot [\boldsymbol{x}^{\mathrm{u}}_{\varepsilon}(p, t+p^{\mathrm{u}}-p) - \bar{\boldsymbol{x}}(p^{\mathrm{u}})] \\ &= [J\boldsymbol{u}(\bar{\boldsymbol{x}}(p^{\mathrm{u}}))] \cdot [\boldsymbol{a} - \boldsymbol{a}] = 0 \,, \end{aligned}$$

by using the streakline property (5). Intuitively, this is because the particle from the steady streakline, *and* that from the unsteady streakline, share the property that they both emanated from the point $\boldsymbol{a}$. The upper limit of t is useful because its insertion leads directly to $M^{\mathrm{u}}(p,t)$, which according to (32) is the correct entity sought in the time-slice t. Thus, multiplying (33) by the integrating factor and integrating from $\tau = t + p^{\mathrm{u}} - p$ to t yields

$$M^{\mathrm{u}}(p,t) = \int_{t+p^{\mathrm{u}}-p}^{t} e^{\int_{\tau}^{t}[\boldsymbol{\nabla}\cdot\boldsymbol{u}](\bar{\boldsymbol{x}}(\xi-t+p))\mathrm{d}\xi} \left[J\boldsymbol{u}\left(\bar{\boldsymbol{x}}(\tau-t+p)\right)\right] \cdot \boldsymbol{v}\left(\bar{\boldsymbol{x}}(\tau-t+p),\tau\right) \mathrm{d}\tau \,. \tag{34}$$

Next, a change of variables $\eta = \tau - t + p$ is applied, and the integral above becomes exactly (8). The interpretation (9), as being the projection in the normal direction to Γ, arises because of (32).

Appendix B. Proof of Theorem 2 [Instantaneous transport].

The proof is based on two observations. First, the displacement $\boldsymbol{x}_\varepsilon^{\mathrm{u}}(p^{\mathrm{d}}, t) - \boldsymbol{b}$, measured along the gate, is from Theorem 1 simply $M^{\mathrm{u}}(p^{\mathrm{d}}, t)/\left|\boldsymbol{u}\left(\bar{\boldsymbol{x}}(p)\right)\right|$ to leading-order. If this is positive, then the dominant velocity across $\mathcal{G}(t)$—which is close to $\boldsymbol{u}\left(\bar{\boldsymbol{x}}(\boldsymbol{b})\right)$—is in the direction of $\hat{\boldsymbol{g}}$, resulting in transport of fluid 2 from $R_2(t)$ to $R_1(t)$. If negative, the flux is of fluid 1 going into $R_2(t)$. Thus, $M^{\mathrm{u}}(p^{\mathrm{d}}, t)$ encodes the sign of the flux. Second, the fluid velocity at all points on $\mathcal{G}(t)$ is to leading-order $\boldsymbol{u}\left(\bar{\boldsymbol{x}}(p)\right)$. This is because in the absence of a velocity agitation the velocity at $\bar{\boldsymbol{x}}(p)$, on $\mathcal{G}$, is $\boldsymbol{u}\left(\bar{\boldsymbol{x}}(p)\right)$, and points normal to $\mathcal{G}$, and moreover both $\mathcal{G}(t)$ and the unsteady velocity agitation have size $\mathcal{O}(\varepsilon)$. Multiplying the velocity across $\mathcal{G}(t)$ by the length of $\mathcal{G}(t)$ therefore gives the instantaneous flux across it; to leading order this is therefore $M^{\mathrm{u}}(p^{\mathrm{d}}, t)$. Thus,

$$\phi(t) = M^{\mathrm{u}}(p^{\mathrm{d}}, t) + \mathcal{O}(\varepsilon^2) =: M(t) + \mathcal{O}(\varepsilon^2)\,.$$

Computing $M(t) = M^{\mathrm{u}}(p^{\mathrm{d}}, t)$ from (8) immediately gives the result.

Acknowledgments. Support from the Australian Research Council through Future Fellowship grant FT130100484 is gratefully acknowledged.

REFERENCES

[1] A. Adjari, *Pumping liquids using asymmetric electrode arrays*, Phys. Rev. E, 61 (2000), pp. R45–R48.
[2] M. Alam, W. Liu, and G. Haller, *Closed-loop separation control: an analytical approach*, Phys. Fluids, 18 (2006), p. 043601.
[3] H. Aref, *Stirring by chaotic advection*, J. Fluid Mech., 143 (1984), pp. 1–21.
[4] S. Balasuriya, *An approach for maximizing chaotic mixing in microfluidic devices*, Phys. Fluids, 17 (2005), p. 118103.
[5] S. Balasuriya, *Direct chaotic flux quantification in perturbed planar flows: general time-periodicity*, SIAM J. Appl. Dyn. Sys., 4 (2005), pp. 282–311.
[6] S. Balasuriya, *Optimal perturbation for enhanced chaotic transport*, Phys. D, 202 (2005), pp. 155–176.
[7] S. Balasuriya, *Cross-separatrix flux in time-aperiodic and time-impulsive flows*, Nonlinearity, 19 (2006), pp. 2775–2795.
[8] S. Balasuriya, *Optimal frequency for microfluidic mixing across a fluid interface*, Phys. Rev. Lett., 105 (2010), p. 064501.
[9] S. Balasuriya, *A tangential displacement theory for locating perturbed saddles and their manifolds*, SIAM J. Appl. Dyn. Sys., 10 (2011), pp. 1100–1126.
[10] S. Balasuriya, *Nonautonomous flows as open dynamical sytems: characterising escape rates and time-varying boundaries*, in Ergodic Theory, Open Dynamics and Structures, Springer, 2014, ch. 1, pp. 1–30.
[11] S. Balasuriya, *Dynamical systems techniques for enhancing microfluidic mixing*, J. Micromech. Microeng., 25 (2015), p. 094005.
[12] S. Balasuriya, *Quantifying transport within a two-cell microdroplet induced by circular and sharp channel bends*, Phys. Fluids, 27 (2015), p. 052005.
[13] S. Balasuriya, *Barriers and transport in unsteady flows: a Melnikov approach*, SIAM Series on Mathematical Modeling and Computation, SIAM Press, Philadelphia, 2016.

[14] S. Balasuriya, *Impulsive perturbations to differential equations: stable/unstable pseudo-manifolds, heteroclinic connections, and flux*, Nonlinearity, 29 (2016), pp. 3897–3933.
[15] S. Balasuriya and M. Finn, *Energy constrained transport maximization across a fluid interface*, Phys. Rev. Lett., 108 (2012), p. 244503.
[16] S. Balasuriya and C. Jones, *Diffusive draining and growth of eddies*, Nonlin. Proc. Geophys., 8 (2001), pp. 241–251.
[17] A. Bassom and A. Gilbert, *The spiral wind-up and dissipation of vorticity and a passive scalar in a strained planar vortex*, J. Fluid Mech., 398 (1999), pp. 245–270.
[18] G. Batchelor, *An introduction to Fluid Dynamics*, Cambridge University Press, Cambridge, 2000.
[19] M. Bazant and T. Squires, *Induced-charge electrokinetic phenomena: Theory and microfluidic applications*, Phys. Rev. Lett., 92 (2004), p. 066101.
[20] F. Bottausci, C. Cardonne, C. Meinhart, and I. Mezić, *An ultrashort mixing length micromixer: the shear superposition micromixer*, Lab Chip, 7 (2007), pp. 396–398.
[21] F. Bottausci, I. Mezić, C. Meinhart, and C. Cardonne, *Mixing in the shear superposition micromixer: three-dimensional analysis*, Proc. Trans. R. Soc. Lond. A, 362 (2004), pp. 1001–1018.
[22] R. Camassa, Z. Lin, R. McLaughlin, L. Mertens, C. Tzou, J. Walsh, and B. White, *Optimal mixing of buoyant jets and plumes in stratified fluids: theory and experiments*, J. Fluid Mech., 790 (2016), pp. 71–103.
[23] R. Chabreyrie, C. Chandre, and N. Aubry, *Complete chaotic mixing in an electro-osmotic flow by destabilization of key periodic pathlines*, Phys. Fluids, 23 (2011), p. 072002.
[24] D. del Castillo Negrete, *Asymmetric transport and non-Gaussian statistics of passive scalars in vortices in shear*, Phys. Fluids, 10 (1998), pp. 576–594.
[25] J. Fernandez, P. Kurowski, P. Petitjeans, and E. Meiburg, *Density-driven unstable flows of miscible fluids in a Hele-Shaw cell*, J. Fluid Mech., 451 (2002), pp. 239–260.
[26] L. Friedland, *Control of Kirchhoff vortices by a resonant strain*, Phys. Rev. E, 59 (1999), pp. 4106–4111.
[27] B. Guo, Z. Zheng, M. Celia, and H. Stone, *Axisymmetric flows from fluid injection into a confined porous medium*, Phys. Fluids, 28 (2016), p. 022107.
[28] G. Haller, *Lagrangian Coherent Structures*, Annu. Rev. Fluid Mech., 47 (2015), pp. 137–162.
[29] P. Hassanzadeh, G. Chini, and C. Doering, *Wall to wall optimal transport*, J. Fluid Mech., 751 (2014), pp. 627–662.
[30] D. Karrasch, *Lagrangian transport through surfaces in volume-preserving flows*, SIAM J. Appl. Math., 76 (2016), pp. 1178–1190.
[31] S. Kida, *Motion of an elliptic vortex in a uniform shear flow*, J. Phys. Soc. Japan, 50 (1981), pp. 3517–3520.
[32] G. Kirchhoff, *Vorlesungen über Mathematische Physik*, vol. 1, Teubner, Leipzig, 1876.
[33] K. Koshel, E. Ryzhov, and V. Zhmur, *Diffusion-affected passive scalar transport in an ellipsoidal vortex in shear flow*, Nonlin. Proc. Geophys., 20 (2013), pp. 437–444.
[34] Y.-K. Lee, C. Shih, P. Tabeling, and C.-M. Ho, *Experimental study and nonlinear dynamic analysis of time-periodic micro chaotic mixers*, J. Fluid Mech., 575 (2007), pp. 425–448.
[35] T. Leweke, S. L. Dizes, and C. Williamson, *Dynamics and instabilities of vortex pairs*, Annu. Rev. Fluid Mech., 48 (2016), pp. 507–541.
[36] C. Lim, Y. Lam, and C. Yang, *Mixing enhancement in microfluidic channel with a constriction under periodic electro-osmotic flow*, Biomicrofluidics, 4 (2010), p. 014101.
[37] Z. Lin, J.-L. Thiffeault, and C. Doering, *Optimal stirring strategies for passive scalar mixing*, J. Fluid Mech., 675 (2011), pp. 465–476.
[38] R. Lynden-Bell, J. Kohanoff, and M. D. Popolo, *Simulation of interfaces between room temperature ionic liquids and other liquids*, Faraday Discussions, 129 (2005), pp. 57–67.
[39] V. Meleshko and G. van Heijst, *On Chaplygin's investigations of two-dimensional vortex structures in an inviscid flow*, J. Fluid Mech., 272 (1994), pp. 157–182.
[40] P. Meunier and E. Villermaux, *How vortices mix*, J. Fluid Mech., 476 (2003), pp. 213–222.
[41] T. Mitchell and L. Rossi, *The evolution of Kirchhoff elliptic vortices*, Phys. Fluids, 20 (2008), p. 054103.
[42] B. Mosovsky and J. Meiss, *Transport in transitory dynamical systems*, SIAM J. Appl. Dyn. Sys., 10 (2011), pp. 35–65.

[43] S. Mula and C. Tinney, *A study of turbulence within a spiralling vortex filament using proper orthogonal decomposition*, J. Fluid Mech., 769 (2015), pp. 570–589.
[44] X. Niu, L. Liu, W. Wen, and P. Sheng, *Active microfluidic mixer chip*, Appl. Phys. Lett., 88 (2006), p. 153508.
[45] T. Peacock, G. Froyland, and G. Haller, *Introduction to focus issue: objective detection of coherent structures*, Chaos, 25 (2015), p. 087201.
[46] A. Poje and G. Haller, *Geometry of cross-stream mixing in a double-gyre ocean model*, J. Phys. Oceanography, 29 (1999), pp. 1649–1665.
[47] P. Roca, A. Cammilleri, T. Duriez, L. Mathelin, and G. Artana, *Streakline-based closed-cloop control of bluff body flow*, Phys. Fluids, 26 (2014), p. 047102.
[48] V. Rom-Kedar, A. Leonard, and S. Wiggins, *An analytical study of transport, mixing and chaos in an unsteady vortical flow*, J. Fluid Mech., 214 (1990), pp. 347–394.
[49] K. Sahu, *Double-diffusive instability in core-annular pipe flow*, J. Fluid Mech., 789 (2016), pp. 830–855.
[50] S. Shadden, *Lagrangian coherent structures*, in Transport and Mixing in Laminar Flows: From Microfluidics to Oceanic Currents, R. Grigoriev, ed., Wiley, Berlin, 2012, pp. 59–89.
[51] K. Shariff, T. Pulliam, and J. Ottino, *A dynamical systems analysis of kinematics in the time-periodic wake of a circular cylinder*, vol. 28 of Lectures in Applied Mathematics, American Mathematical Society, 1991, pp. 613–646.
[52] H. Song, Z. Cai, H. Noh, and D. Bennett, *Chaotic mixing in microchannels via low frequency switching transverse electroosmotic flow generated on integrated microelectrodes*, Lab Chip, 10 (2010), pp. 734–740.
[53] A. Souza and C. Doering, *Maximal transport in the Lorenz equations*, Phys. Lett. A, 379 (2015), pp. 518–523.
[54] M. Stremler and B. Cola, *A maximum entropy approach to optimal mixing in a pulsed source-sink flow*, Phys. Fluids, 18 (2006), p. 011701.
[55] A. Stroock, S. Dertinger, A. Adjari, I. Mezić, H. Stone, and G. Whitesides, *Chaotic mixer for microchannels*, Science, 295 (2002), pp. 647–651.
[56] R. Sturman and S. Wiggins, *Eulerian indicators for predicting and optimizing mixing quality*, New J. Phys., 11 (2009), p. 075031.
[57] M. Sussman, P. Smereka, and S. Osher, *A level set approach for computing solutions to incompressible 2-phase flow*, J. Comput. Phys., 114 (1994), pp. 146–159.
[58] P. Tabeling, M. Chabart, A. Dodge, C. Jullien, and F. Okkels, *Chaotic mixing in cross-channel micromixers*, Phil. Trans. R. Soc. Lond. A, 362 (2004), pp. 987–1000.
[59] J.-L. Thiffeault, *Using multiscale norms to quantify mixing and transport*, Nonlinearity, 84 (2012), pp. R1–R44.
[60] M. Turner, *Temporal evolution of vorticity staircases in randomly strained two-dimensional vortices*, Phys. Fluids, 26 (2014), p. 116603.
[61] C. Y. Wang, *Exact solutions of the steady-state Navier-Stokes equations*, Annu. Rev. Fluid Mech., 23 (1991), pp. 159–177.
[62] S. Wang, Z. Jiao, X. Huang, C. Yang, and N. Nguyen, *Acoustically induced bubbles in a microfluidic channel for mixing enhancement*, Microfluid Nanofluid, 6 (2009), pp. 847–852.
[63] T. Weinkauf and H. Theisel, *Streak lines as tangent curves of a derived vector field*, IEEE Trans.Visualization Comput. Graphics, 16 (2010), pp. 1225–1234.
[64] S. Wiggins, *Chaotic Transport in Dynamical Systems*, Springer-Verlag, New York, 1992.
[65] Y. Young, H. Tufo, A. Dubey, and R. Rosner, *On the miscible Rayleigh-Taylor instability: two and three dimensions*, J. Fluid Mech., 447 (2001), pp. 377–408.
[66] Z. Zheng, L. Rongy, and H. Stone, *Viscous fluid injection into a confined channel*, Phys. Fluids, 27 (2015), p. 062105.
[67] V. Zhmur, E. Ryzhov, and K. Koshel, *Ellipsoidal vortex in a nonuniform flow: dynamics and chaotic advections*, J. Marine Res., 69 (2011), pp. 435–461.
[68] E. Ziemniak, C. Jung, and T. Tél, *Tracer dynamics in open hydrodynamical flows as chaotic scattering*, Phys. D, 76 (1994), pp. 123–146.